ELSEVIER

Nuclear Physics A 627 (1997) 645–678

NUCLEAR PHYSICS A

Pion and kaon photoproduction at high energies: forward and intermediate angles

M. Guidal [1], J.-M. Laget [2], M. Vanderhaeghen [3]

CEA/Saclay, DAPNIA-SPhN, F-91191 Gif-sur-Yvette Cedex, France

Received 15 April 1997; revised 10 October 1997; accepted 28 October 1997

Abstract

A model for high energy pion and kaon photoproduction ($E_\gamma \gtrsim 4$ GeV) is presented which interpolates between the low and higher momentum transfer regions. At low momentum transfer (which is described in terms of Regge trajectory exchanges), the model is able to give an economical description of unpolarized and polarized data for both the charged and neutral pion photoproduction reactions as well as for $K^+\Lambda$ and $K^+\Sigma$ photoproduction data, available at high energy. At higher momentum transfer, an extrapolation based on saturating Regge trajectories, and which satisfies scaling laws at asymptotically large transfers, is found able to describe the few existing $\gamma p \to n\pi^+$ data. The model can be used as a guidance to interpret forthcoming data at larger momentum transfers. © 1997 Elsevier Science B.V.

PACS: 13.60.Le; 12.40.Nn; 12.38.Bx

Keywords: Pseudoscalar meson photoproduction; High energy; Regge theory; High momentum transfer reactions

1. Introduction

The study of meson photoproduction at intermediate energy ($E_\gamma \gtrsim 4$ GeV) and momentum transfer becomes now experimentally accessible in a systematic way with the high duty cycle electron facilities like TJNAF. In particular, the combination of the large acceptance detector CLAS and the high intensity beam of TJNAF, makes possible

[1] Present address: NIKHEF, Kruislaan 409, P.O. Box 41882, 1009 DB Amsterdam, The Netherlands, e-mail: michelg@nikhef.nl.

[2] E-mail: laget@phnx7.saclay.cea.fr,

[3] E-mail: marcvdh@phnx7.saclay.cea.fr.

PII S0375-9474(97)00612-X

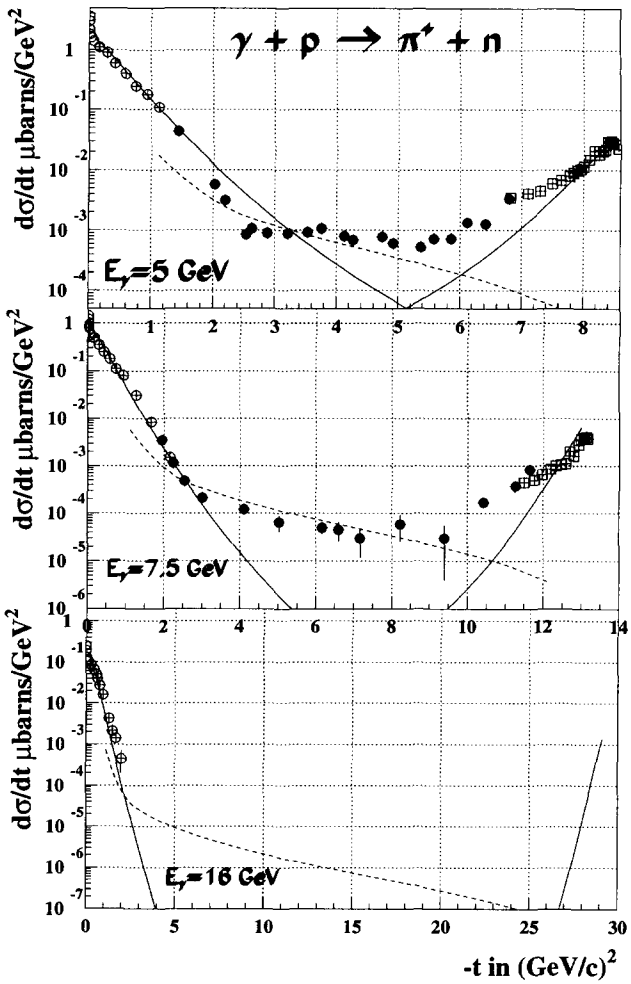

Fig. 1. Differential cross sections of the $\gamma p \rightarrow n\pi^+$ reaction. Solid lines: "soft" model based on linear Regge trajectories in the t-channel (mesons) and u-channel (baryons). Dashed lines: "hard" model based on saturating meson Regge trajectories. The data at low t are from Ref. [1], the data at low u are from Ref. [2] whereas the high p_T data are from Ref. [3].

the study of meson photo- and electroproduction reactions at large angle and opens up a virgin unexplored field.

In this paper the pion and kaon photoproduction reactions on the nucleon at high energies are studied at forward angles and an extrapolation is given towards larger momentum transfer. For these reactions, a model is presented which starts from a description in terms of Regge trajectory exchanges at forward angles. The large pseudoscalar meson photoproduction data set which exists at high energy and low momentum transfer, allows to put severe tests on the theoretical model. Subsequently, we extend the model to the higher momentum transfer region by using saturating trajectories. Fig. 1 summarizes the results for the $\gamma p \rightarrow n\pi^+$ differential cross section. At energies above $E_\gamma \gtrsim 4$ GeV,

the experimental differential cross sections for pseudoscalar meson photoproduction reactions exhibits a strongly collimated peak at forward ($|t| \lesssim 2$ GeV^2) and backward ($|u| \lesssim 1$ GeV^2) angles, corresponding to the exchange of mesons in the t-channel and baryons in the u-channel respectively. Regge theory [4,5] permits to give a simple and natural description of the smooth energy and angular dependence ($s^{2\alpha(t)-2}$ at forward angles, $s^{2\alpha(u)-2}$ at backward angles) of these peaks, where s, t and u are the Mandelstam variables of the reaction and where $\alpha(t)$ and $\alpha(u)$ are the exchanged trajectories. At large momentum transfer, around 90°, the data show a plateau in t and satisfy scaling laws in s, which can be reproduced by saturating Regge trajectories.

The main results of the model for the charged pion photoproduction reactions were presented in a previous letter [6]. The present paper focusses on the complete development of the model.

In Section 2 the formalism for pseudoscalar meson photoproduction at forward angles and intermediate/high energies is outlined in its technical details. Special attention is paid to the implementation of gauge invariance which is crucial in the description of both unpolarized and polarized observables. A comparison with the large amount of data at forward angles for both charged and neutral pion photoproduction provides us with a stringent check of the theoretical inputs. A discussion of available models in the literature is also given.

In Section 3 the same formalism as for $\gamma N \to \pi N$ is extended to the $\gamma p \to K^+ \Lambda$ and $\gamma p \to K^+ \Sigma^\circ$ photoproduction reactions and the model is compared with the available data at forward angles and high energies.

An extrapolation to larger momentum transfer of the Regge model for the pion photoproduction reaction is presented in Section 4. It is based on the introduction of saturating trajectories and hadronic form factors for the outgoing particles so as to be consistent with the scaling laws at large momentum transfer. This transition region at larger momentum transfer holds promise to investigate how a description in terms of hadronic degrees of freedom through effective hadronic Lagrangians at low momentum transfer is connected to a description in terms of quarks and gluons within the domain of perturbative QCD (pQCD) at large momentum transfer.

2. Pion photoproduction

2.1. Formalism

In this section we concentrate on forward angles and base our model on the exchange of dominant meson Regge trajectories in the t-channel. Starting from a standard Feynman diagram formalism as in Ref. [7], we take into account the exchange of a Regge trajectory (which represents the exchange of a *family* of particles with the same internal quantum numbers) by replacing the usual pole-like Feynman propagator of a *single* particle (i.e. $1/(t-m^2)$, where m is the mass of the exchanged particle) by a so-called Regge propagator, while keeping the vertex structure given by the Feynman diagrams

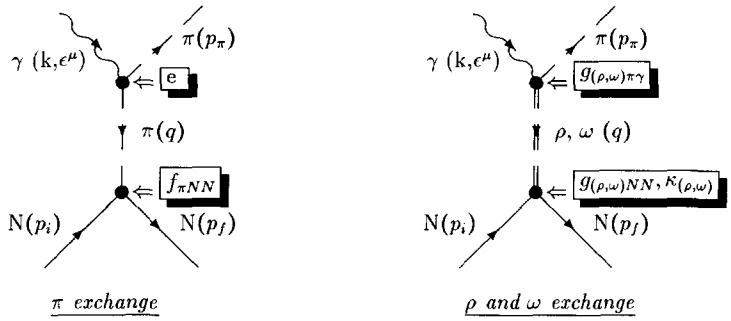

Fig. 2. t-channel Feynman diagrams considered in the model. At forward angles: π, ρ and ω exchanges. At backward angles: nucleon and Δ exchanges. The coupling constants involved are displayed at the corresponding vertices.

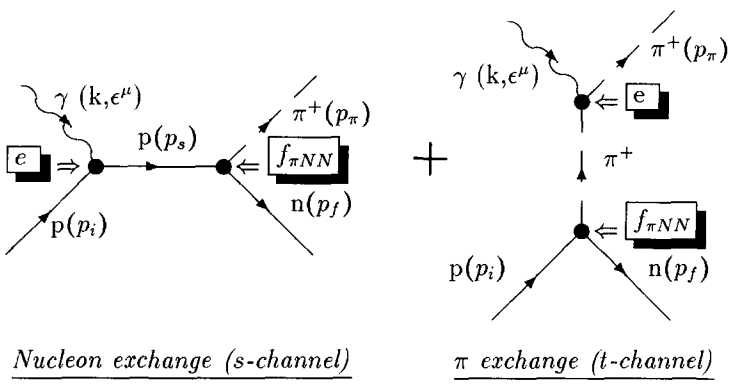

Fig. 3. The sum of the two diagrams (when using PS coupling) is gauge invariant for the $\gamma p \to n\pi^+$ reaction. The individual diagrams are not.

which correspond to the first materialization of the trajectory. Such a procedure is similar to the one adopted in Ref. [8].

In the case of the pion photoproduction reaction, we aim at a simultaneous description of the four channels $\gamma p \to n\pi^+$, $\gamma p \to p\pi^0$, $\gamma n \to p\pi^-$ and $\gamma n \to n\pi^0$. The dominant exchanges in this model are, for forward charged pion photoproduction the π and ρ trajectories and for forward neutral pion photoproduction the ρ and ω trajectories. The corresponding Feynman diagrams are shown on Fig. 2.

We decompose the amplitude in the following way:

$$\mathcal{M}_{fi} = \epsilon_\mu \cdot J^\mu , \tag{1}$$

where J^μ is the hadronic current operator containing the dynamical information on pion photoproduction.

The expressions for the hadronic current operators below are derived from effective Lagrangians which have been used by numerous authors ([7–12] to cite recent papers). In the following expressions, the isospin factor is indicated between curly brackets. We also define the electric charge $e > 0$ ($e^2/4\pi = 1/137$) and the four-momenta $q = k - p_\pi$

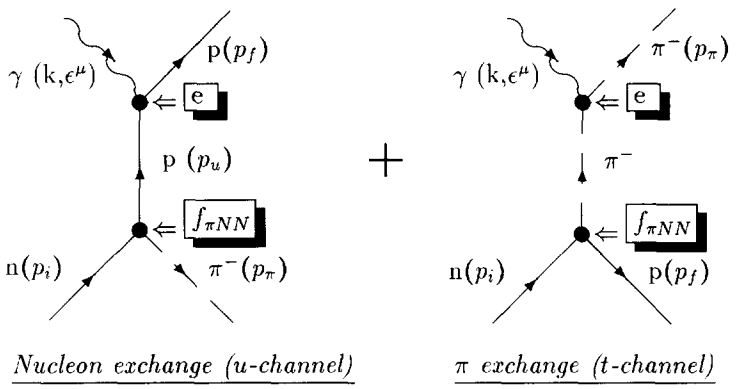

Fig. 4. The sum of the two diagrams is gauge invariant for the $\gamma n \rightarrow p\pi^-$ reaction. The individual diagrams are not.

and $p_u = p_f - k$ ($q^2 = t$ and $p_u^2 = u$). Throughout this work, we follow the conventions of Bjorken and Drell [13].

- π (0^-) exchange (contributes only to charged pion photoproduction):

$$\left\{ \begin{array}{l} J^{\mu}_{\pi t-\mathrm{exch}}(\gamma p \rightarrow n\pi^+) \\ J^{\mu}_{\pi t-\mathrm{exch}}(\gamma n \rightarrow p\pi^-) \end{array} \right\} = -i \left\{ \begin{array}{c} \sqrt{2} \\ -\sqrt{2} \end{array} \right\} e \frac{f_{\pi NN}}{m_\pi} \bar{N}_f (q - p_\pi)^\mu \mathcal{P}^{\{0\}} \not{q} \gamma^5 N_i \,, \quad (2)$$

where $\mathcal{P}^{\{0\}} = 1/(q^2 - m_\pi^2)$ is the propagator of a spin 0 particle and $f_{\pi NN}$ is the pion–nucleon coupling constant: $f^2_{\pi NN}/4\pi = 0.08$ ([14]).

- ρ (1^-) exchange:

$$\left\{ \begin{array}{l} J^{\mu}_{\rho}(\gamma p \rightarrow n\pi^+) \\ J^{\mu}_{\rho}(\gamma p \rightarrow p\pi^0) \end{array} \right\} = \left\{ \begin{array}{l} J^{\mu}_{\rho}(\gamma n \rightarrow p\pi^-) \\ -J^{\mu}_{\rho}(\gamma n \rightarrow n\pi^0) \end{array} \right\}$$

$$= - \left\{ \begin{array}{c} \sqrt{2} \\ 1 \end{array} \right\} e \frac{g_{\rho\pi\gamma}}{m_\pi} g_{\rho NN} \bar{N}_f \varepsilon^{\nu\mu\rho\alpha} k_\nu q_\rho \mathcal{P}^{\{1\}}_{\alpha\beta}$$

$$\times \left[\gamma^\beta + \kappa_\rho i\sigma^{\beta\lambda} \frac{q_\lambda}{2m_N} \right] N_i \,, \quad (3)$$

where

$$\mathcal{P}^{\{1\}}_{\alpha\beta} = \frac{1}{q^2 - m_\rho^2} \left[-g_{\alpha\beta} + \frac{q_\alpha q_\beta}{m_\rho^2} \right]$$

is the propagator of a spin 1 particle. One can omit the term $q_\alpha q_\beta / m_\rho^2$ of the propagator because it cancels by contraction with the antisymmetric tensor $\varepsilon^{\nu\mu\rho\alpha} q_\rho$. $g_{\rho NN}$ and κ_ρ are the strong coupling constants of the ρNN vertex and $g_{\rho\pi\gamma}$ is the coupling

constant of the electromagnetic vertex $\rho\pi\gamma$. This latter constant can be derived from the electromagnetic decay width of the ρ:

$$\Gamma_{(\rho\to\pi\gamma)} = \frac{\alpha}{24}\left[\frac{g_{\gamma\pi\rho}}{m_\pi}\right]^2 m_\rho^3 \left[1-\left(\frac{m_\pi}{m_\rho}\right)^2\right]^3 , \tag{4}$$

so that $g_{\rho^\pm\pi\gamma} = 0.103$ with $\Gamma_{(\rho\to\pi\gamma)} = 67.95$ keV [15]. Several values for the strong coupling constants of the ρ can be found in the literature ("strong" ρ [14] and "weak" ρ [16,10,12]). In this work the values for a "strong" ρ coupling were adopted: $g^2_{\rho NN}/4\pi = 0.92$, $\kappa_\rho = 6.1$ (values taken from Ref. [14], Table 8). We found that they give a better description of the charged pion photoproduction data.

- ω (1^-) exchange (contributes only to neutral pion photoproduction):

$$\begin{aligned} J^\mu_{\omega\pi\gamma}(\gamma p \to p\,\pi^0) &= J^\mu_{\omega\pi\gamma}(\gamma n \to n\,\pi^0) \\ &= -e\frac{g_{\omega\pi\gamma}}{m_\pi} g_{\omega NN}\bar{N}_f \varepsilon^{\nu\mu\rho\alpha} k_\nu q_\rho \mathcal{P}^{\{1\}}_{\alpha\beta} \\ &\quad \times \left[\gamma^\beta + \kappa_\omega i\sigma^{\beta\lambda}\frac{q_\lambda}{2m_N}\right] N_i , \end{aligned} \tag{5}$$

$\mathcal{P}^{\{1\}}_{\alpha\beta}$ is the spin 1 propagator as defined above, $g_{\omega NN}$ and κ_ω are the strong coupling constants of the ωNN vertex and $g_{\omega\pi\gamma}$ is the coupling constant of the electromagnetic vertex $\omega\pi\gamma$. Similarly to Eq. (4), $g_{\omega\pi\gamma} = 0.314$ with $\Gamma_{(\omega\to\pi\gamma)} = 720$ keV [15]. The strong coupling constant of the ω is constrained within the range : $15 \lesssim g^2_{\omega NN}/4\pi \lesssim 20$, $\kappa_\omega \approx 0$ [14]. In this work we will use $g_{\omega NN} = 15$ as this gives a good description of the π^0 observables as will be shown further on.

- b_1 (1235) (1^+) exchange (contributes in principle to charged *and* neutral pion photoproduction, but will be needed here only for neutral pion photoproduction as will be justified in the section on the results):

$$\begin{aligned} J^\mu_{b_1}(\gamma p \to p\,\pi^0) &= -J^\mu_{b_1}(\gamma n \to n\,\pi^0) \\ &= -e\frac{g_{b_1\pi\gamma}}{m_\pi}\bar{N}_f((k\cdot q)g^{\mu\alpha} - q^\mu k^\alpha)\mathcal{P}^{\{1\}}_{\alpha\beta} g_{b_1NN} \\ &\quad \times \left[\gamma^\beta\gamma^5 + \frac{\kappa_{b_1}}{2m_N}\not{q}\gamma^\beta\gamma^5\right] N_i , \end{aligned} \tag{6}$$

$\mathcal{P}^{\{1\}}_{\alpha\beta}$ is the spin 1 propagator as defined above, g_{b_1NN} and κ_{b_1} are the strong coupling constants of the b_1NN vertex and $g_{b_1\pi\gamma}$ is the coupling constant of the electromagnetic vertex $b_1\pi\gamma$. For charged pions, the coupling constant $g_{b_1^\pm\pi\gamma}$ can be deduced from the radiative decay width $\Gamma_{(b_1^\pm\to\pi^\pm\gamma)} = 223$ keV [15]. This yields $g_{b_1^\pm\pi\gamma} = 0.086$ using a formula similar to Eq. (4). For the strong coupling constant g_{b_1NN}, there is no precise value available in the literature. The only observable where b_1 exchange is necessary (photon asymmetry Σ for $\gamma p \to p\pi^0$) will allow us to estimate the product of the b_1 coupling constants.

Having specified the vertices, we now give the expressions of the Regge propagators for the meson trajectories of the π, ρ, ω and b_1. The idea behind replacing the usual pole-

like Feynman propagator by a Regge propagator is to *economically* take into account the exchange of high-spin and high-mass particles in the t- (and u-) channel(s) which cannot be neglected any more as one goes to higher energies. It has already been followed by Levy, Majerotto and Read [8].

The Regge trajectories are of the form $\alpha(t) = \alpha_0 + \alpha' * t$. The precise numerical values we have taken for the coefficients α_0 and α' of the different trajectories will be indicated in the section dealing with the results of the model (Section 2.3).

- π (0^-) exchange:

$$\frac{1}{t-m_\pi^2} \Longrightarrow \mathcal{P}^{\pi}_{\text{Regge}} = \left(\frac{s}{s_0}\right)^{\alpha_\pi(t)} \frac{\pi\alpha'_\pi}{\sin(\pi\alpha_\pi(t))} \frac{\mathcal{S}_\pi + e^{-i\pi\alpha_\pi(t)}}{2} \frac{1}{\Gamma(1+\alpha_\pi(t))}, \tag{7}$$

- ρ (1^-) exchange:

$$\frac{1}{t-m_\rho^2} \Longrightarrow \mathcal{P}^{\rho}_{\text{Regge}} = \left(\frac{s}{s_0}\right)^{\alpha_\rho(t)-1} \frac{\pi\alpha'_\rho}{\sin(\pi\alpha_\rho(t))} \frac{\mathcal{S}_\rho + e^{-i\pi\alpha_\rho(t)}}{2} \frac{1}{\Gamma(\alpha_\rho(t))}, \tag{8}$$

- ω (1^-) exchange:

$$\frac{1}{t-m_\omega^2} \Longrightarrow \mathcal{P}^{\omega}_{\text{Regge}} = \left(\frac{s}{s_0}\right)^{\alpha_\omega(t)-1} \frac{\pi\alpha'_\omega}{\sin(\pi\alpha_\omega(t))} \frac{\mathcal{S}_\omega + e^{-i\pi\alpha_\omega(t)}}{2} \frac{1}{\Gamma(\alpha_\omega(t))}, \tag{9}$$

- b_1 (1^+) exchange:

$$\frac{1}{t-m_{b_1}^2} \Longrightarrow \mathcal{P}^{b_1}_{\text{Regge}} = \left(\frac{s}{s_0}\right)^{\alpha_{b_1}(t)-1} \frac{\pi\alpha'_{b_1}}{\sin(\pi\alpha_{b_1}(t))} \frac{\mathcal{S}_{b_1} + e^{-i\pi\alpha_{b_1}(t)}}{2} \frac{1}{\Gamma(\alpha_{b_1}(t))}, \tag{10}$$

In these expressions, s_0 is a mass scale which is conventionally taken as $s_0 = 1$ GeV^2 [4] and $\mathcal{S} = \pm 1$ is the signature of the trajectory. The gamma function $\Gamma(\alpha(t))$ suppresses poles of the propagator in the unphysical (scattering) region. As is well known from Regge theory [4], trajectories can be either non-degenerate or degenerate. A degenerate trajectory is obtained by adding or subtracting the non-degenerate trajectories of Eqs. (7) and (8) with the two opposite signatures. This leads to degenerate trajectories which have either a rotating ($e^{-i\pi\alpha(t)}$) or a constant (1) phase. We will indicate the scheme of degeneracy we follow during the discussion of the results (Section (2.3)). The Regge propagators of Eqs. (7) to (10) have the property that they reduce to the Feynman propagators $1/(t-m^2)$ if one approaches the first pole on the trajectory (i.e. $t \to m^2$). This means that the farther we go from the pole, the more the result of our model will differ from conventional Feynman diagram based models.

Summarizing, whereas usual Regge models rely on the FIT of (t- or s-channel) helicity amplitudes as a sum of Regge poles and cuts, the advantage of our approach is that the only parameters involved are the coupling constants at the vertices of the first materialization of the trajectories with the external particles ($f_{\pi NN}$, $g_{\rho NN}$, κ_ρ, $g_{\rho\pi\gamma}$,...): they are well-known from the numerous and precise studies and analyses in the resonance region.

2.2. Gauge invariance

In this approach in terms of Feynman diagrams, it is well known that the t-channel π diagram alone does not satisfy electromagnetic gauge invariance by itself. For the $\gamma p \to n\pi^+$ reaction, it has to be complemented by the s-channel nucleon diagram (when using pseudoscalar (PS) coupling) or by the s-channel nucleon diagram and the Kroll–Rudermann contact diagram (when using pseudovector (PV) coupling) to arrive at a gauge invariant amplitude. The two coupling schemes lead to exactly the same gauge invariant amplitude as both nucleons are on-shell. Similarily, for the $\gamma n \to p\pi^-$ reaction, the t-channel π-diagram has to be complemented by the u-channel nucleon exchange diagram (when using PS coupling) to satisfy gauge invariance. These relations between the Born terms is fundamental, it ensures that the electric charge is conserved (the ρ, ω and b_1 exchange diagrams are gauge invariant by themselves).

How to incorporate these additional gauge restoring terms in our Regge model? Regge theory deals essentially with t-channel exchanges, it is a priori not "*natural*" to introduce a s-channel diagram in this framework. When reggeizing the t-channel π-exchange diagram ($J^{\mu}_{\pi t-\text{exch}}$) as in Eq. (7), the gauge invariance has to be implemented by reggeizing the s (or u)-channel nucleon diagram in the same way as the t-channel π-exchange diagram. When we reggeized the t-channel π-exchange diagram, we have actually multiplied the usual Feynman t-channel diagram (with the traditional Feynman pole-like propagator $1(t-m_\pi^2)$) by the factor $P_{\text{Regge}} \cdot (t-m_\pi^2)$. Applying the same procedure for the s (or u)-channel diagrams, one obtains symbolically:

$$\mathcal{M}_\pi(\gamma p \to \pi^+ n) \to \mathcal{M}_{\pi\, t-\text{exch}} + (t-m_\pi^2)(\mathcal{P}^{\pi}_{\text{Regge}}) \cdot \mathcal{M}^{s-\text{channel } N}, \tag{11}$$

$$\mathcal{M}_\pi(\gamma n \to \pi^- p) \to \mathcal{M}_{\pi\, t-\text{exch}} + (t-m_\pi^2)(\mathcal{P}^{\pi}_{\text{Regge}}) \cdot \mathcal{M}^{u-\text{channel } N}. \tag{12}$$

This leads to the following gauge invariant reggeized π-exchange current operators:

$$J^{\mu}_{\pi}(\gamma p \to n\pi^+) \to -i\left\{\sqrt{2}\right\} e \frac{f_{\pi NN}}{m_\pi} \bar{N}_f \times \left[(q-p_\pi)^{\mu} \not{q}\gamma^5 - 2m_N(t-m_\pi^2)\gamma^5 \frac{(\not{p}_s + m_N)}{s-m_N^2}\gamma^{\mu}\right] N_i \mathcal{P}^{\pi}_{\text{Regge}}, \tag{13}$$

$$J^{\mu}_{\pi}(\gamma n \to p\pi^-) \to i\left\{\sqrt{2}\right\} e \frac{f_{\pi NN}}{m_\pi} \bar{N}_f \times \left[(q-p_\pi)^{\mu} \not{q}\gamma^5 + 2m_N(t-m_\pi^2)\gamma^{\mu} \frac{(\not{p}_u + m_N)}{u-m_N^2}\gamma^5\right] N_i \mathcal{P}^{\pi}_{\text{Regge}}. \tag{14}$$

The second term in Eq. (13) (resp. Eq. (14)) can be interpreted as the electric part of the s-channel (resp. u-channel) nucleon exchange contribution when using PS πNN coupling and where one uses a pointlike γNN coupling. We have kept for the s-channel diagram the minimum necessary term to restore gauge invariant, i.e. the electric part coupling. It is well known that the (anomalous) magnetic part is gauge invariant by

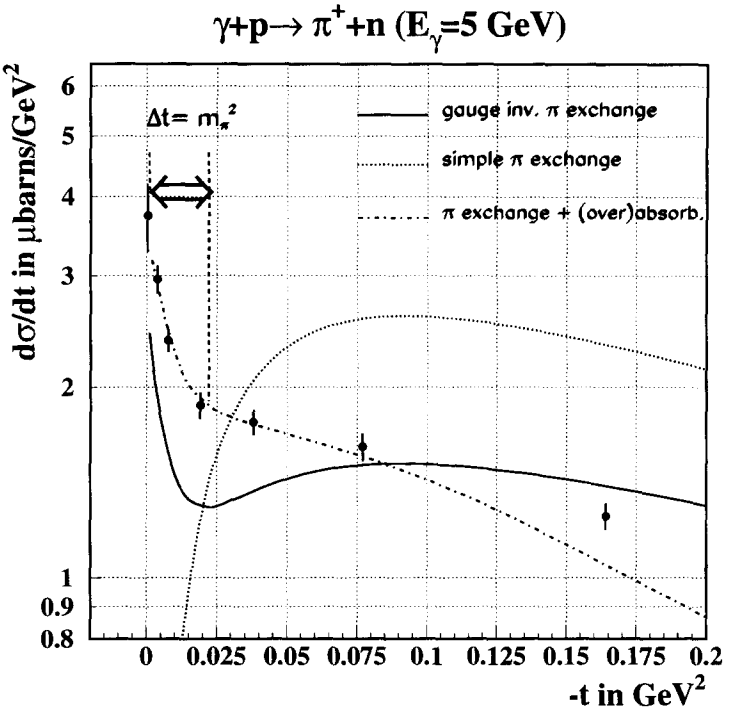

Fig. 5. Sharp rise at very forward angles ($\Delta t \approx m_\pi^2$) of $d\sigma/dt(\gamma p \to \pi^+ n)$. A comparison is given between a model based on a simple t-channel π-exchange diagram (dashed curve), a model based on this same diagram but with overabsorption – with fit value $C = 2.1$, see text – (dashed-dotted curve) and the gauge invariant model based on t-channel π-exchange and the s-channel nucleon exchange diagrams (solid curve). The data are from Ref. [1].

itself. We have also implemented it however, by sake of completeness, and we found its influence negligeable anyway. It is therefore preferable to keep this minimal scheme of gauge restoration. This interpretation does of course not imply that one reggeizes all s-channel (resp. u-channel) exchanges in addition to t-channel exchanges which would violate duality. This particular s-channel (u-channel) "diagram" (being a Born term), is an indissociable part of the t-channel π-exchange and is imposed by charge conservation. Indeed a gauge can be found [17] where the contribution from the π-exchange t-channel diagram vanishes and where consequently the nucleon pole graph produces a π-pole in the cross section! It is therefore a natural choice to reggeize it by multiplying with $\mathcal{P}^{\pi}_{\text{Regge}} \cdot (t - m_\pi^2)$ as this is exactly the same factor which enters when reggeizing the t-channel diagram of Eq. (11). This implementation of gauge invariance ensures that one recovers the result obtained for the Born diagrams if one is close to the pion pole ($t \to m_\pi^2$), as $\mathcal{P}^{\pi}_{\text{Regge}} \cdot (t - m_\pi^2) \to 1$ for $t \to m_\pi^2$. This implementation of gauge invariance is one new feature of the present model compared to various previous works on pion photoproduction and turns out to be crucial to obtain a good description of asymmetries and to describe the π^-/π^+ ratio as will be shown in the next section.

The introduction of the s (u) -channel diagram has an immediate effect on the

forward differential cross-section of the reaction $\gamma p \to n\pi^+$ ($\gamma n \to p\pi^-$): it creates a sharp rise at very forward angles over a range $\Delta t \approx {m_\pi}^2$ (Fig. 5). This feature was also found within the context of the Electric Born Term Model [17,18] (where one implements only Born diagrams), which however cannot explain the energy and exponential t-dependence of the differential cross section which are reproduced through the reggeization in our model.

It is well known that the t-channel π exchange diagram alone goes to zero for $t \to 0$. Traditionally, Regge analyses explained this forward peak in pion exchange reactions (both by electromagnetic and hadronic probes) as being due to absorption corrections [19]. We present on Fig. 5 the result of such a model based on a standard absorption prescription:

$$\mathcal{M}^I_{i\to f} = \mathcal{M}^I_{\text{pole}} \left(1 - Ce^{-l^2/As}\right) . \tag{15}$$

It must be emphasized that these absorption models rely on the fit of a free parameter C, the "strength" of the absorption effect: here, its value has to be taken $C = 2.1$ in order to fit the data, which is a value which is in agreement with most other studies (see Refs. [20,21] for instance). Although leading to a quantitatively very satisfactory fit, this value of C greater than 1 (usually referred to as "overabsorption") induces however an unphysical sign reversal of the lowest partial waves instead of absorbing them. Also, at larger angles ($t \approx -0.5$ GeV^2), it produces a dip in the differential cross section (originating from the destructive interference of the cut and the pole), a structure which is not observed in charged pion photoproduction. Overall, these absorption models do not respect gauge invariance which is a fundamental constraint for electromagnetic induced reactions.

The question can then be raised: what is the origin of the narrow sharp peak observed at very forward angles in charged pion photoproduction? Is it due to absorption/rescattering effects as commonly explained? Or is it a deep manifestation of gauge invariance through the s-channel nucleon exchange diagram? Or is it just an artefact of our gauge invariance prescription? We will see in the next section when we review and investigate all the existing pion photoproduction data at forward angles that we will clearly be able to favor the "gauge invariance" point of view. In spite of the light quantitative disagreement that can be observed on Fig. 5, we will be able to conclude that "gauge invariance" is the main effect at the origin of the rise of the differential cross section at very forward angles. Rescattering effects might also be present (which could explain – through "weak" absorption – the remaining discrepency with the data at very forward angles) but are not dominant.

2.3. Results and discussion

We will now compare the results of our model with all the existing data for the four reactions of photoproduction of pion on the nucleon: $\gamma p \to n\pi^+$, $\gamma n \to p\pi^-$, $\gamma p \to p\pi^0$: and $\gamma n \to n\pi^0$. Each channel has its own characteristics and a simultaneous

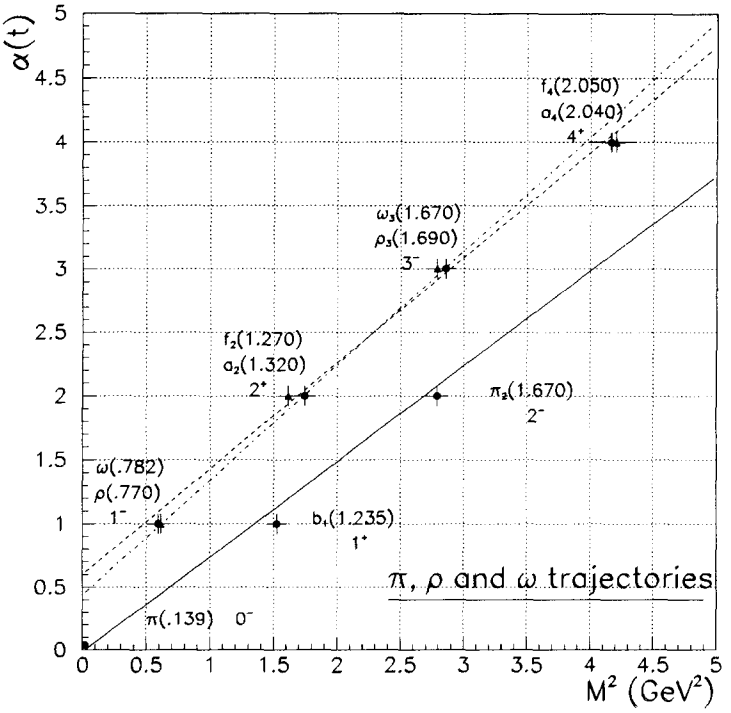

Fig. 6. π, ρ and ω meson trajectories used in the model.

description of such a broad data set, where the *same* trajectories or coupling constants contribute to *different* channels, imposes severe constraints and leaves very little freedom.

We recall that in our approach the only parameters involved are the coupling constants at the vertices of the first materialization of the trajectories with the external particles, as the trajectory equations are determined from the Chew–Frautschi plots. For pion photoproduction, the parameters involved are well known or at least strongly constrained from the numerous and precise studies and analyses in the resonance region. Their values and the appropriate references will be given below.

2.3.1. $\gamma p \rightarrow n\pi^+$

Fig. 7 shows the forward differential cross section for the four photon energies E_γ = 5, 8, 11, 16 GeV. The dominant trajectories which can possibly contribute to this reaction are the π's and the ρ's.

There is no dip in the differential cross section as far as the data go and we naturally take degenerate trajectories. We take the well established value of the πNN coupling constant: $f^2_{\pi NN}/4\pi = 0.08$. For the ρ, two sets of values for the coupling constants are used in the literature which are known as a "weak" ρ and a "strong" ρ. The weight of the π being determined, a strong ρ is here needed to explain the magnitude of the cross section. We adopt the values given by [14]:

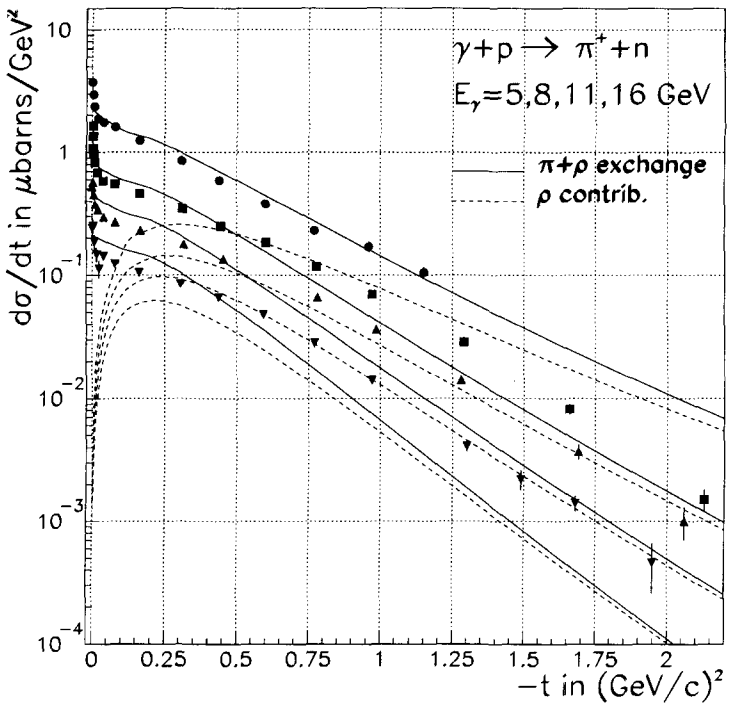

Fig. 7. Differential cross section for the $\gamma p \rightarrow n\pi^+$: reaction for the four photon energies E_γ = 5, 8, 11, 16 GeV (upper data and curves correspond with E_γ = 5 GeV, whereas the lower ones with E_γ = 16 GeV). Gauge invariant $\pi + \rho$ exchange model (full curves), ρ-exchange contribution (dashed curves). The data are from Ref. [1].

$$\frac{g^2_{\rho NN}}{4\pi} = 0.92\,, \tag{16}$$

$$\kappa_\rho = 6.1\,. \tag{17}$$

The equations of the π and ρ trajectories are given by

$$\alpha_\pi(t) = 0.7(t - m_\pi^2)\,, \tag{18a}$$

$$\alpha_\rho(t) = 0.55 + 0.8t\,, \tag{18b}$$

and are displayed on Fig. 6. The energy dependence of the cross section shown in Fig. 7 is well reproduced: it is experimentally proportional to E_γ^{-2}, a dependence which is common to all photoproduction processes at forward angles at high energies. In the framework of a Regge model, the energy dependence of the forward differential cross section follows the form:

$$\frac{d\sigma}{dt} \propto s^{2\alpha(0)-2}\,. \tag{19}$$

An intercept approximatively equal to 0 is therefore appropriate. This gives support to the dominance of the pion trajectory at forward angles (by comparison with the ρ whose intercept is close to 0.5). We recall that the dominance of the π at very forward

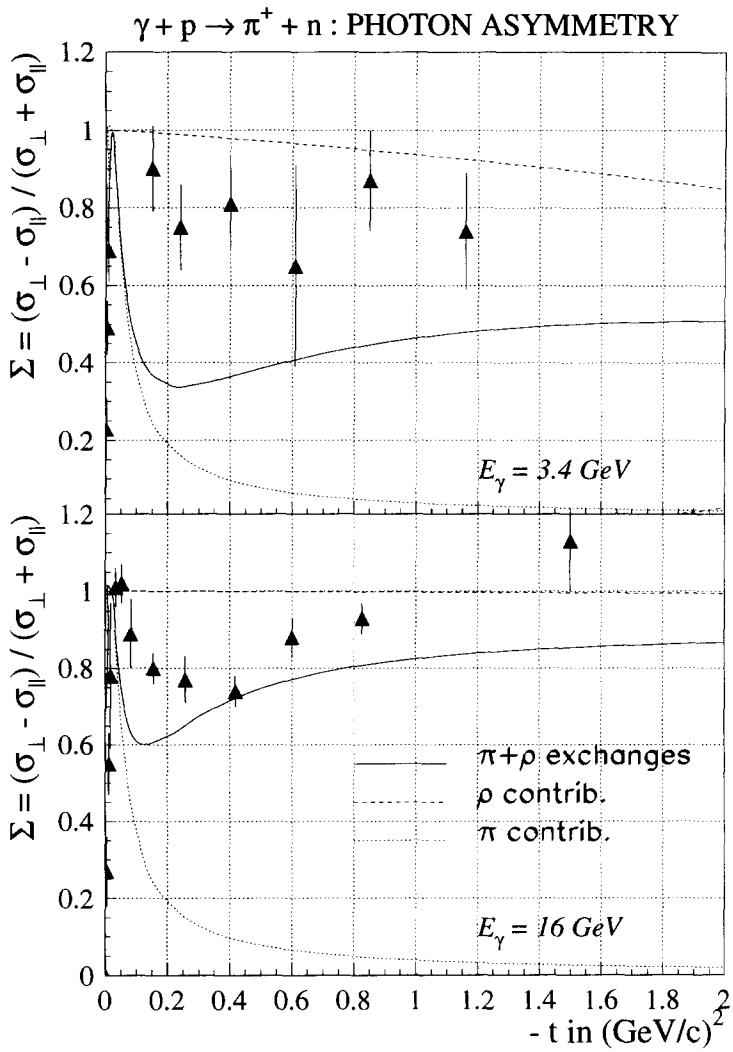

Fig. 8. Photon asymmetry for $\gamma p \rightarrow n\pi^+$. Data are from Ref. [22] (3.4 GeV) and Refs. [23,24] (16 GeV).

angle is due to the s-channel nucleon exchange diagram which produces the sharp rise at extreme forward angles. The ρ becomes dominant at higher transfers and becomes more important as the photon energy increases due to its higher intercept.

The photon asymmetry data for this reaction are displayed on Fig. 8. As on Fig. 5, we observe here again a rapid rise at low $-t$ up to $\approx +1$ in the region $\Delta t \approx m_\pi{}^2$. This is also naturally explained in the present model by the reggeized s-channel nucleon diagram, which guaranties the gauge invariance of the model. This observable provides a strong argument in favor of our approach. Indeed, if the gauge restoring term in Eq. (13) was not present, the asymmetry would be -1 at very forward angles as it is well known [18] that unnatural parity exchange (like simple t-channel π-exchange) leads to

an asymmetry of -1 at low $-t$. Introducing (over)absorption effects would not modify this fact. The electric term of the s-channel nucleon exchange diagram contributes in equal part to $\sigma_{\parallel}$ and $\sigma_{\perp}$ and by interference with the t-channel pion exchange diagram provides an asymmetry of $+1$ at very forward angles where the influence of the diagram is dominant. Beyond the region $\Delta t \approx {m_\pi}^2$, the role of s-channel diagram diminishes and the asymmetry decreases also. At larger values of $-t$, the asymmetry rises to $+1$, which points to the dominance of the ρ-exchange (natural parity exchange) as can also be seen in Fig. 7 from the differential cross section. The s-channel diagram provides here a natural explanation of the photon asymmetry observable in the very forward region which cannot be reproduced simply in any absorption model.

We show in Fig. 9 the target asymmetry data. We can make three remarks with respect to this observable. First, the fact that this asymmetry is non-zero confirms that there are indeed *at least* two trajectories (the π and ρ) contributing to our process. Polarisation is indeed always due to an interference term: a single Feynman diagram does not produce any *nucleon* (target or recoil) asymmetry.

Secondly, the gauge invariance is also crucial to reproduce the target asymmetry. The interference of the t-channel ρ-exchange diagram with the simple t-channel π-exchange diagram produces only a very weak asymmetry. The large value for the target asymmetry comes from the interference with the s-channel diagram.

Lastly, the negative sign of the target asymmetry directly reflects the relative signs between the π and ρ exchange diagrams which is well known [14].

As a conclusion of this subsection devoted to the reaction $\gamma p \rightarrow n\pi^+$, the detailed examination of the polarization observables (photon asymmetry and target polarization) have clearly shown the critical role of the implementation of gauge invariance. Whereas the sharp rise at very forward angles of the differential cross section could as well be explained (and quantitatively in a better way) by absorption/rescattering effects, this is not the case for the polarization observable where we would get absolutely opposite behaviors to the data without the introduction of the s-channel diagram in Eq. (13) to restore gauge invariance.

2.3.2. $\gamma n \rightarrow p\pi^-$

There are two measured observables for negative charged pion photoproduction:
- The ratio $\mathcal{R}$ of the differential cross sections $d\sigma(\gamma n \rightarrow p\pi^-)/d\sigma(\gamma p \rightarrow n\pi^+)$,
- The photon asymmetry Σ.

Fig. 10 shows the experimental ratio $d\sigma(\gamma n \rightarrow p\pi^-)/d\sigma(\gamma p \rightarrow n\pi^+)$ which is characterized by a strong negative curvature at low t ($\mathcal{R} \lesssim 0.3$ at $t \approx -0.3$ GeV^2). This observable has always been a challenge to explain in numerous models. Indeed, the parameters (i.e exchanged trajectories – π and ρ – and the coupling constants) for $\gamma n \rightarrow p\pi^-$ are the same than for $\gamma p \rightarrow n\pi^+$. There is in principle only a change of sign of the isospin coefficient of the t-channel pion exchange diagram. Therefore, there is no additional degree of freedom and any model explaining $\gamma p \rightarrow n\pi^+$ must describe as well $\gamma n \rightarrow p\pi^-$.

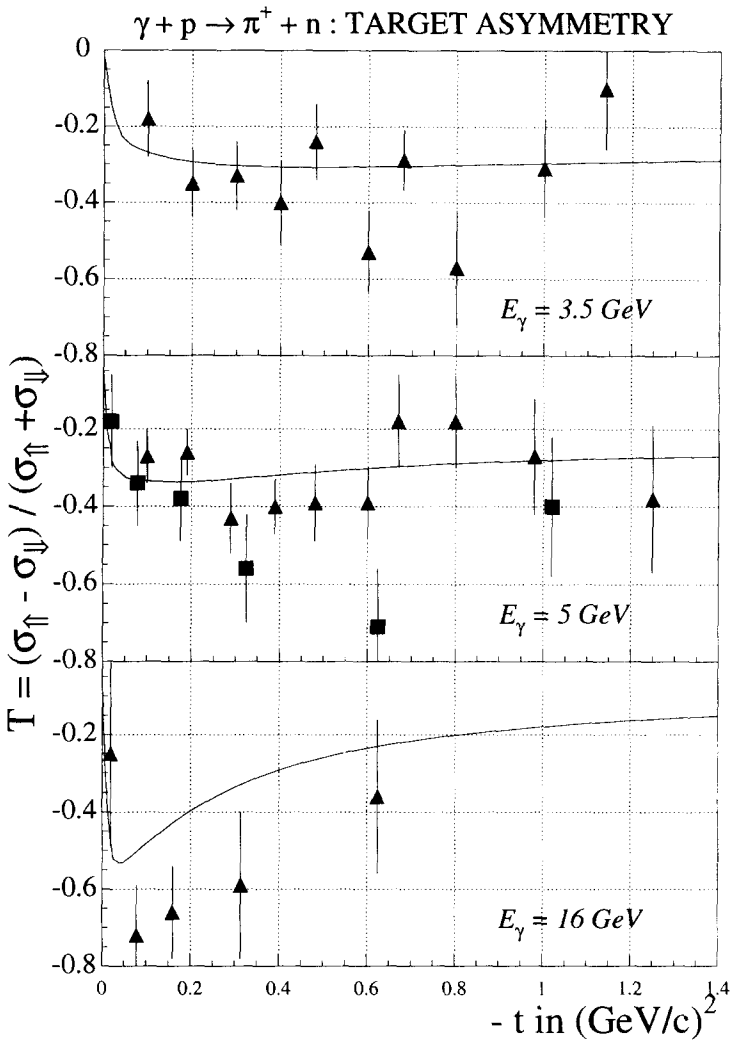

Fig. 9. Target asymmetry for $\gamma p \rightarrow n\pi^+$. Data are from Ref. [25] (3.5 and 5 GeV) and Ref. [26] (5 and 16 GeV).

The succesful description of this observable by our model relies on two points. First, as explained in Section 2.1, the concern of gauge invariance has led us to adjoin the s-channel nucleon exchange diagram to the t-channel pion exchange diagram for $\gamma p \rightarrow n\pi^+$. Similarly, the u-channel nucleon exchange diagram complements the t-channel pion exchange diagram for $\gamma n \rightarrow p\pi^-$. The Reggeized u-channel diagram in $\gamma n \rightarrow p\pi^-$ plays a similar role than the s-channel diagram in $\gamma p \rightarrow n\pi^+$ and produces a sharp rise at very forward angles in the $\gamma n \rightarrow p\pi^-$ differential cross section. Consequently, the ratio is close to 1 at very forward angles and the "sharp rises" in the $\Delta t \approx m_\pi{}^2$ region are of the same magnitude.

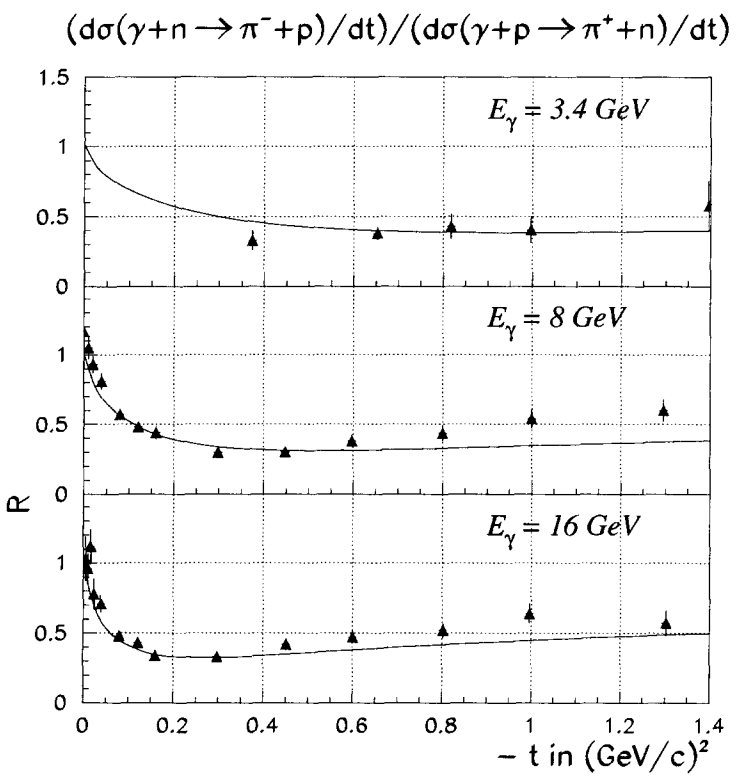

Fig. 10. Ratio $\mathcal{R}$ of the differential cross sections: $\frac{d\sigma}{dt}(\gamma n \to p\pi^-) \Big/ \frac{d\sigma}{dt}(\gamma p \to n\pi^+)$. The data are from Ref. [27] (3.4 GeV) and Ref. [28] (8 GeV and 16 GeV).

The second point is proper to Regge theory and is related to the degeneracy schemes of the trajectories. If we consider degenerate trajectories, we have two ways of "degenerating" them, with a *constant* phase or a *rotating* phase:

$$\beta(t)\left[(e^{-i\pi\alpha(t)}+1) \pm (e^{-i\pi\alpha(t)}-1)\right] = 2\beta(t) \begin{cases} 1\,, \\ e^{-i\pi\alpha(t)}\,. \end{cases} \tag{20}$$

G-parity consideration imposes then that:

- The ρ has positive G-parity, therefore it couples *similarly* to the $\gamma\pi^+\rho^-$ and $\gamma\pi^-\rho^+$ vertices.
- The a_2 has negative G-parity, therefore there is a *negative relative sign* between the $\gamma\pi^+a_2^-$ and $\gamma\pi^-a_2^+$ couplings.
- The π has negative G-parity, therefore it couples *with a negative relative sign* to the $\gamma\pi^+\pi^-$ and $\gamma\pi^-\pi^+$ vertices.
- The b_1 has positive G-parity, therefore it couples *similarily* to the $\gamma\pi^+b_1{}^-$ and $\gamma\pi^-b_1{}^+$ vertices.

The difference between $\gamma p \to n\pi^+$ and $\gamma n \to p\pi^-$ is precisely the exchanges of a π^+ and a ρ^+ in one case and a π^- and a ρ^- in the other. This translates into the following

schemes of degeneracy for the π-b_1 and ρ-a_2 trajectories, in a schematic notation:

$$\frac{d\sigma}{dt}(\gamma p \to \pi^+ n) \propto |(\pi + b_1) + (\rho + a_2)|^2 , \tag{21a}$$

$$\frac{d\sigma}{dt}(\gamma n \to \pi^- p) \propto |-(\pi - b_1) + (\rho - a_2)|^2 , \tag{21b}$$

where the pion comes with the opposite sign in both reactions (cfr. isospin dependence of Eq. (2)). More explicitely, Eqs. (21aa) and (21bb) are written as:

$$\frac{d\sigma}{dt}(\gamma p \to \pi^+ n) \propto |\mathcal{M}_\pi e^{-i\pi\alpha_\pi(t)} + \mathcal{M}_\rho e^{-i\pi\alpha_\rho(t)}|^2 , \tag{22a}$$

$$\frac{d\sigma}{dt}(\gamma n \to \pi^- p) \propto |-\mathcal{M}_\pi \cdot 1 + \mathcal{M}_\rho \cdot 1|^2 , \tag{22b}$$

where $\mathcal{M}_\pi$ and $\mathcal{M}_\rho$ are the π^+ production amplitudes (without the Regge phase) corresponding with the exchange of a π or ρ trajectory respectively. G-parity considerations thus lead to rotating phase for the π and ρ trajectories in the $\gamma p \to n\pi^+$ process and to a constant phase in the $\gamma n \to p\pi^-$ process. The result on the ratio $\mathcal{R}$ as shown in Fig. 10 is striking and constitutes a remarkable success for the model. The good description of this ratio $\mathcal{R}$ in the present model follows from both the use of degenerate trajectories and the implementation of gauge invariance: this is a new feature of our model compared to previous works. It was found that this ratio is difficult to reproduce in other frameworks than Regge theory as the degeneracy concern is essential. The power of Regge theory comes from the *economic* way (with no additional free parameters as coupling constants for instance) with which it takes into account the exchange of *heavy* particles. It is indeed the "heavy" mesons b_1 and a_2 which are at the base of the effect through their relation to the lighter mesons π and ρ of the same trajectory.

The photon asymmetry (Fig. 11) for $\gamma n \to p\pi^-$ is completely similar to the $\gamma p \to n\pi^+$ one. The sharp rise in the $\Delta t \approx m_\pi{}^2$ region finds again a the natural explanation in the presence of the u-channel nucleon exchange diagram needed to respect gauge invariance.

For the comparison with existing approaches in the literature, we compare with Ref. [29] where a recent analysis was made (and where references to older work can be found). In Ref. [29], two models were used to describe charged pion photoproduction data at high energies and at forward angles. A so-called "minimal model" where only Regge pole contributions are retained and a pion cut which is needed to reproduce the forward spike. As can be seen from the resulting fits and as is stated in Ref. [29], this "minimal model" is not very accurate at a quantitative level as it underestimates the π^+ differential cross section data even at modest t-values, it gives a too large value for the π^-/π^+ ratio and the description of the asymmetries is rather poor. An improved fit of the data was given in Ref. [29] by including more parameters which were allowed to vary and by including other cut contributions. With this "full model" of Ref. [29], a good fit of charged pion photoproduction could be obtained at low momentum transfer however at the expense of some 30 fit parameters. The model we presented arrives at a rather good description of the same data without cuts and without relying on a large

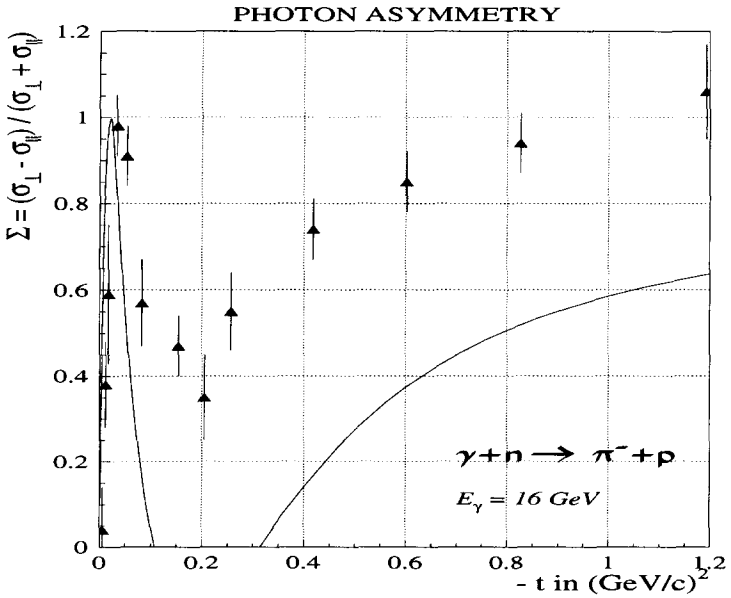

Fig. 11. Photon asymmetry for the reaction $\gamma n \rightarrow p\pi^-$. The data are from Ref. [23].

number of fit parameters as in Ref. [29]. This result is already interesting in itself. As is explained in the Letter for charged pion photoproduction, this is basically due to our implementation of gauge invariance and to the use of degenerate trajectories which gives the correct π^-/π^+ ratio. Besides giving an economical description of low-t charged pion photoproduction data, we show below that this model is also able to give a description of neutral pion photoproduction and of the charged kaon photoproduction data. Furthermore it will be shown how the model can be extended to larger momentum transfer which is outside the domain of applicability of all previous Regge fit models.

2.3.3. $\gamma p \rightarrow p\pi^0$

The only trajectories which can be exchanged in this channel are the ω and ρ ones. The pion, with zero charge and spin, cannot contribute. The ω and ρ trajectory intercepts are comparable $\alpha_0 \approx 0.5$ GeV^{-2}) but the values of the coupling constants $g_{\omega NN}$ and $g_{\omega\pi\gamma}$ make the ω contribution dominant. The coupling constants of the ρ have been introduced in the subsection devoted to the $\gamma p \rightarrow n\pi^+$ reaction (2.3.1) and for the ω we will take $g_{\omega NN} = 15$ and $\kappa_\omega = 0$ in agreement with the limits of the literature [7].

The main characteristic of the $\gamma p \rightarrow p\pi^0$ differential cross section is the presence of a dip for $|t| \approx 0.6$ GeV^2 (Fig. 12). Such dips appear in numerous other reactions (as well with electromagnetic as with hadronic probes) and there are two main explanations in the literature of the mechanisms giving rise to these structures: "Wrong signature zeroes" and absorption/rescattering processes. In this latter option the dips arise from the destructive interference between Regge poles and cuts. However, this approach requires "strong" cuts (overabsorption, i.e. $C > 1$) in order to produce a strong enough interference. As we have clearly discarded in the previous sections the notion of strong absorption

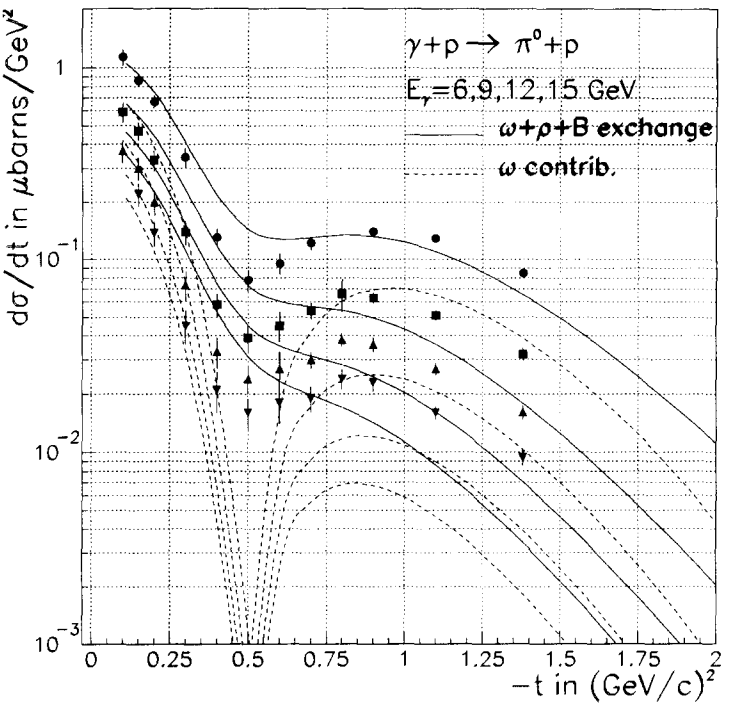

Fig. 12. Differential cross section for the reaction $\gamma p \rightarrow p\pi^0$ for the four photon energies $E_\gamma = 6, 9, 12, 15$ GeV. Data are from Ref. [30].

processes, we will rely on the "wrong signature process" mechanism to generate dips in the differential cross section. In particular the dip occuring at $t = -0.6$ GeV^2 for $\gamma p \rightarrow p\pi^0$ can be explained by the zero of the ω trajectory: $\alpha_\omega(-0.6) = 0$. The ω trajectory is shown in Fig. 6 and its expression is given by:

$$\alpha_\omega(t) = 0.44 + 0.9t\,. \tag{23}$$

To be consistent with $\gamma p \rightarrow n\pi^+$ and $\gamma n \rightarrow p\pi^-$, we will keep the ρ trajectory degenerate. It will also fill in a bit the dip resulting from the zero of the ω trajectory which would be too deep otherwise.

For the reaction $\gamma p \rightarrow p\pi^0$ data are available for the three simple polarization observables Σ, T and P.

The ω has *natural* parity (like the ρ) and therefore contributes mainly to $\sigma_\perp$. It is then not surprising to observe a photon asymmetry predominantly equal to 1 (Fig. 13). However, the slight dip at $t \approx -0.6$ GeV^2 is not compatible with the exchange of the ω and ρ trajectories alone. A trajectory of *unnatural* parity must take part in the process so to decrease the asymmetry down to $\approx$0.7 in the dip region where the ω does not contribute but the ρ remains. As the pion cannot contribute, the trajectory of unnatural parity with a high enough intercept has to be the b_1. There are very few constraints on the coupling constants of the b_1. This is the only place in this discussion on pion photoproduction at forward angles, where we are forced to allow for a "real"

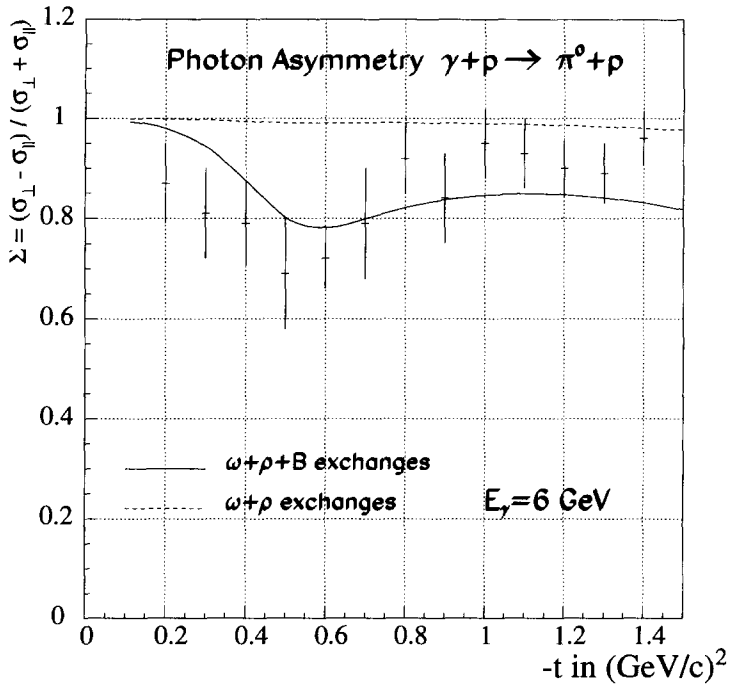

Fig. 13. Photon asymmetry for the reaction $\gamma p \rightarrow p\pi^0$. The data are from Ref. [31].

free parameter to estimate the necessary influence of the b_1 in the photon asymmetry Σ of $\gamma p \rightarrow p\pi^0$. This parameter is the product of the coupling constants $g_{b_1\pi\gamma} \cdot g_{b_1 NN}$ using the current operator of Eq. (6). Fitting the Σ asymmetry, in order to obtain a value close to 0.7 in the dip region at $t \approx -0.6$ GeV^2, we find $g_{b_1^0\pi\gamma} \cdot g_{b_1 NN} = 2$ (we have taken the tensor coupling $\kappa_{b_1} = 0$ in the fit). As the radiative decay of the b_1^0 has not been measured, we use the isospin relation (which is very well verified for the ρ meson) to estimate $g_{b_1^0\pi\gamma} = \sqrt{2} g_{b_1^\pm\pi\gamma}$. Putting in the value $g_{b_1^\pm\pi\gamma} = 0.086$ found before, the above fit yields as value for the $b_1 NN$ coupling constant $g_{b_1 NN} = 16.44$ which is of the same order as the strong coupling constant $g_{\omega NN}$ ($g_{\omega NN} = 15$). We have taken the same trajectory equation for the b_1 as for the π. We might also remark that the presence in the dip of a *natural* parity trajectory (i.e. the ρ) is necessary because otherwise the asymmetry Σ would drop to -1 due to the contribution of the b_1 alone. This gives support to our choice of a degeneracy scheme for the ρ trajectory.

The influence of the b_1 on the differential cross section is negligible even in the dip where the ρ is still dominant. The presence of the b_1 shows only through the Σ asymmetry where it is clearly necessary. The fact that our model relies on very few "ingredients" (two trajectories for $\gamma p \rightarrow n\pi^+$ and $\gamma n \rightarrow p\pi^-$, three in the neutral pion case) allows to clearly separate and distinguish the role and influence of each contribution. Each structure or effect in an observable can thus be identified with a simple origin (i.e here the b_1 explains the dip in the asymmetry).

The target and recoil polarization must be equal as the target and recoil baryons are the

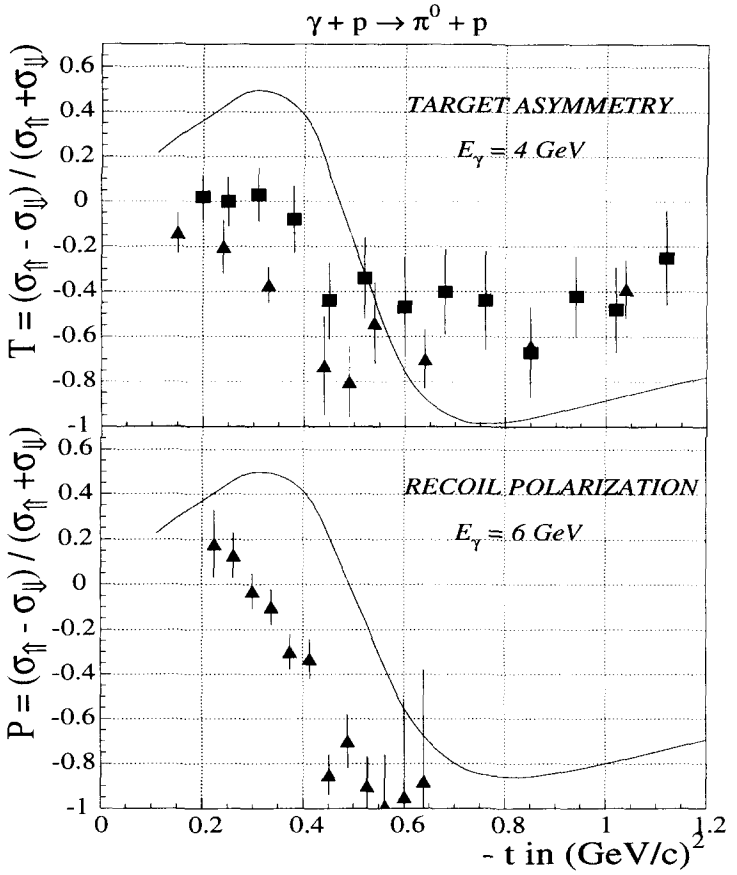

Fig. 14. Target asymmetry (T) and recoil polarization (P) for the reaction $\gamma p \rightarrow p\pi^0$. The data are from Ref. [32] (▲) and Ref. [33] (■) for T and from Ref. [34] for P.

same (i.e. the proton). Within the large experimental error bars, this is indeed the case as can be seen from Fig. 14. Here again, the polarization results from the interference between the ρ and ω contributions. The change of sign in P and T which occurs at $t \approx -0.3$ GeV^2 experimentally and at $t \approx -0.6$ GeV^2 in our model (corresponding to a change of phase of the ω contribution for $\alpha_\omega(t) = 0$) is a natural characteristic of a "wrong signature zero". It seems very difficult to explain this "node" in the framework of an absorption model if this latter mechanism is at the origin of the dip in the differential cross section.

2.3.4. $\gamma n \rightarrow n\pi^0$

The only measured observable for this reaction is the ratio of the differential cross section $\mathcal{R}$ (Fig. 15):

$$\mathcal{R} = \frac{d\sigma(\gamma n \rightarrow n\pi^0)}{d\sigma(\gamma p \rightarrow p\pi^0)}. \tag{24}$$

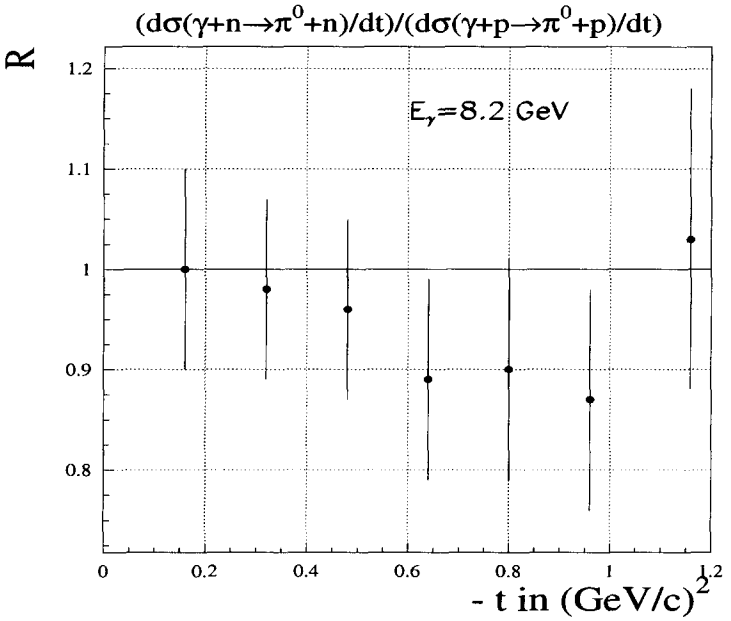

Fig. 15. Ratio $\mathcal{R}$ of the differential cross sections: $d\sigma(\gamma n \to n\pi^0)/d\sigma(\gamma p \to p\pi^0)$. The data are from Ref. [35].

The G-parity considerations exposed in (2.3.2) do not apply for this channel as the exchanged particles ρ and ω are neutral. Thus, they participate *similarly* to the two reactions $\gamma p \to p\pi^0$ and $\gamma n \to n\pi^0$. It has to be concluded that the ratio $\mathcal{R}$ can only be equal to 1. The data of Fig. 15 support this argument.

3. Kaon photoproduction

3.1. Theoretical approach

The extension of our model of forward pion photoproduction to the strangeness sector is straightforward. The spins of the particle involved are similar and the same Feynman diagrams have to be considered. The dominant meson trajectories are the K and the $K^*(890)$ (Fig. 17) who have respectively the spin-parities of the pion (0^-) and of the ρ (1^-). The only modifications with respect to the currents given in Section 2.1 are the coupling constants involved and the isopin factors which are all equal to 1. As for the case of pion photoproduction, the s- and u- channel diagrams (with only the electric term) are of course also included in order to ensure gauge invariance with respect to the t-channel K exchange diagram (Fig. 16).

Forward kaon photoproduction has also been studied theoretically in the past by Levy et al. [8]. Their approach is similar to ours based on the reggeization of Feynman diagrams. However, an essential difference is that they rely on the notions of

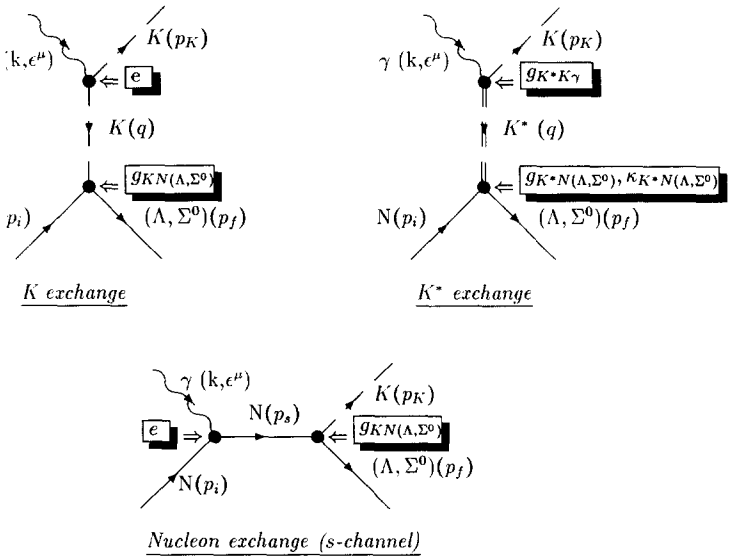

Fig. 16. Feynman diagrams considered for the reactions $\gamma p \rightarrow K^+\Lambda$ and $\gamma p \rightarrow K^+\Sigma$. At forward angles: exchange of the K and K^* trajectories. The s-channel nucleon exchange diagram is necessary so that the t-channel K-exchange diagram is gauge invariant.

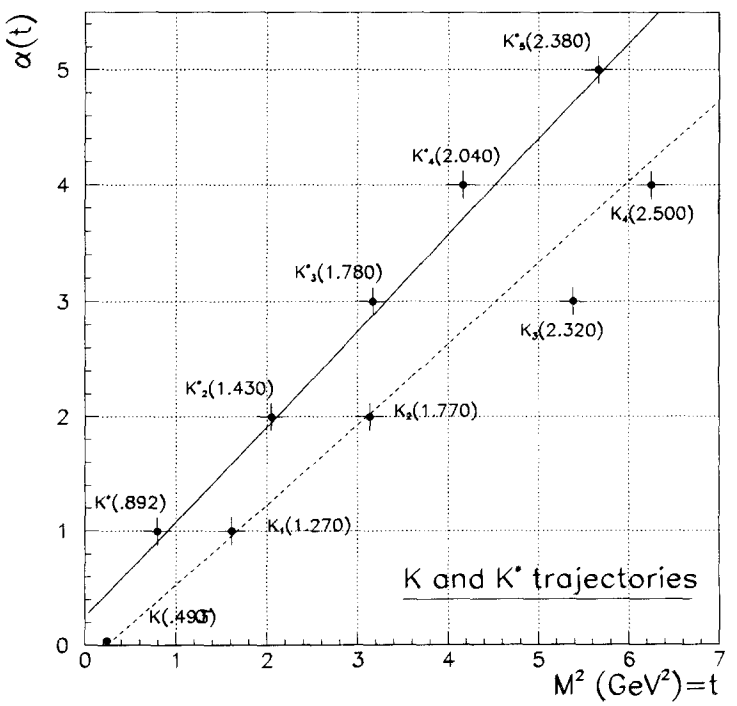

Fig. 17. K and K^* meson trajectories.

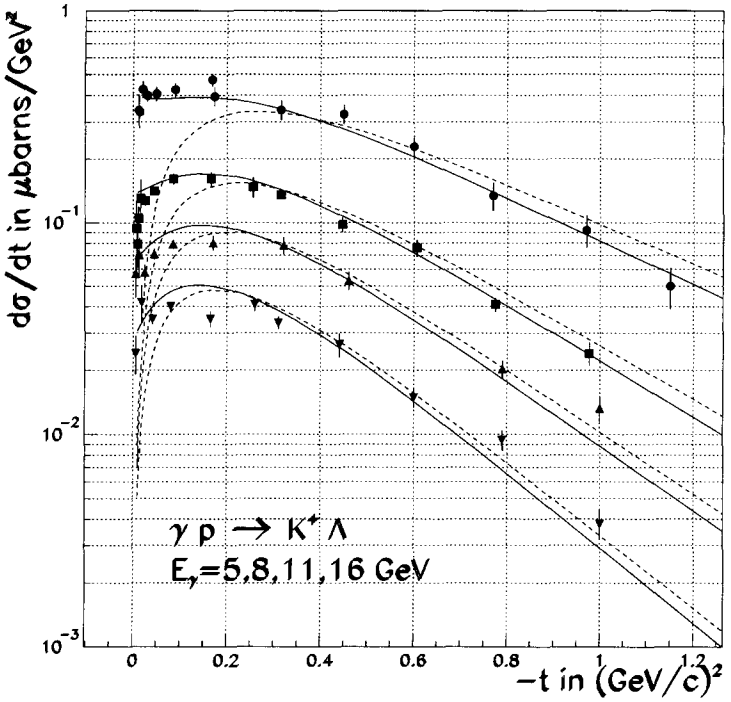

Fig. 18. Differential cross section for the reaction $\gamma p \rightarrow K^+\Lambda$ for the four photon energies $E_\gamma = 5, 8, 11, 16$ GeV. Gauge invariant $K + K^*$ exchange model (full curves), K^*-exchange contribution (dashed curves). The data are from Ref. [41].

(over)absorption to explain the data. As a consequence, their model is not gauge invariant as is stated in their article and as a side effect, gives rise to dips in the differential cross section at larger $-t$ which are not observed experimentally. Again, we will show that it is not necessary to introduce these absorption/rescattering effects to describe the data and that a simple and elegant explanation is provided by our gauge invariant model.

Figs. 18 and 19 show the forward differential cross sections for the four photon energies $E_\gamma = 5, 8, 11, 16$ GeV for Λ and Σ photoproduction respectively. There is no apparent structure in the data so we will take the trajectories of the K and K^* degenerate for the two reactions. As previously, the normalization of our amplitudes are given by the coupling constants at the vertices of the Feynman diagrams. The constants at the electromagnetic vertices are the electric charge for the K exchange diagram and $g_{\gamma KK^*}$ for the K^* exchange diagram. This latter constant can simply be estimated through the electromagnetic decay width of the K^*:

$$\Gamma_{(K^{*+}\rightarrow K\gamma)} = \frac{\alpha}{24}\left[\frac{g_{\gamma KK^*}}{M}\right]^2 m_{K^*}^3 \left[1 - \left(\frac{m_K}{m_K^*}\right)^2\right]^3 , \tag{25}$$

where M is a mass scale (that we take equal to 1 GeV) to make the coupling constant $g_{\gamma KK^*}$ dimensionless. With $\Gamma_{(K^{*+}\rightarrow K\gamma)} = 0.05$ MeV, one easily derives:

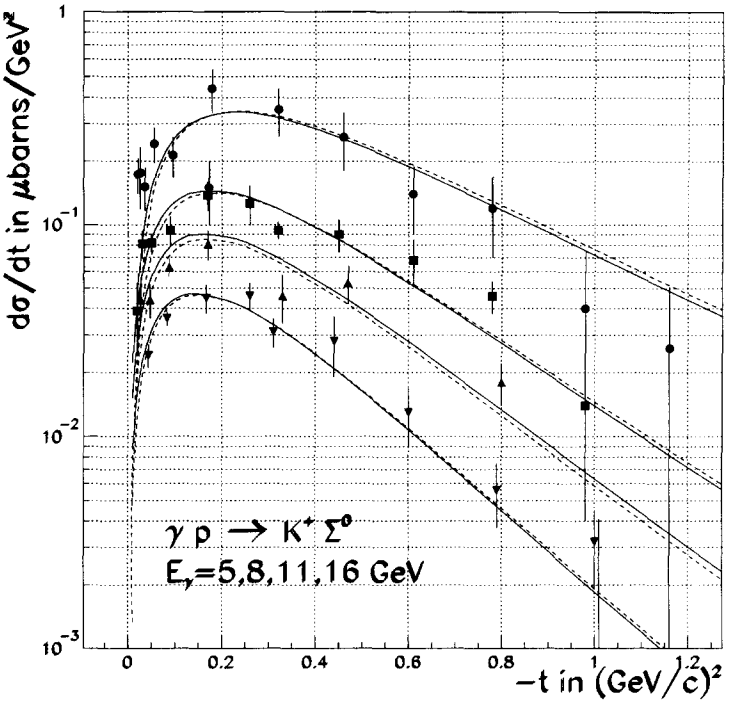

Fig. 19. Differential cross section for the reaction $\gamma p \rightarrow K^+\Sigma$ for the four photon energies $E_\gamma = 5, 8, 11, 16$ GeV. Same curve conventions as in Fig. 18. The data are from Ref. [41].

$$g_{\gamma KK^*} = 0.842\,. \tag{26}$$

The strong coupling constants involved are $g_{K(\Lambda,\Sigma)N}$ (for the K exchange) and $g_{K^*(\Lambda,\Sigma)N}$ and $\kappa_{K^*(\Lambda,\Sigma)N}$ (for the K^* exchange). Here, the situation is different from pion photoproduction as these coupling constants are much less well known or constrained experimentally. Firstly, the abundance and precision of the experimental data for the NN and πN scattering reactions allows fine analyses of the nucleon potential from which the π, ρ and ω contributions can be extracted and therefore their respective coupling constants. Experimental access to the *hyperon*–nucleon interaction is much more difficult and does not permit such precise analyses. Secondly, in contrast to the resonances in the pion photoproduction reaction, the Λ and Σ are states below kaon threshold, which complicates the extraction of their couplings as there are several contributions already just above threshold. Furthermore, most isobaric models [36–39] which try to describe low energy kaon photoproduction are non-unitary. Despite the lack of experimental constraints and the approximations of the isobaric models for kaon photoproduction, there is an alternative (theoretical) way to estimate these coupling constants: through the SU(3) symmetry.

SU(3) permits to link the coupling constants $g_{K\Lambda N}$ and $g_{K\Sigma N}$ to the well established constant $g_{\pi NN}$ through the α_D coefficient:

$$g_{K\Lambda N} = -\frac{1}{\sqrt{3}} g_{\pi NN}(3 - 2\alpha_D)\,, \tag{27}$$

$$g_{K\Sigma N} = -g_{\pi NN}(1 - 2\alpha_D)\,. \tag{28}$$

The coefficient α_D is known as the symmetric coupling fraction due to the fact that their are two octet representations in SU(3); a symmetric and an anti-symmetric one. The numerical value of α_D is relatively well determined: SU(6) predicts $\alpha_D = \frac{3}{5}$ but we will rather use the experimental value $\alpha_D = 0.644 \pm 0.009$ [40]. Then, taking $\frac{g^2_{\pi NN}}{4\pi} = 14.4$ (corresponding to $\frac{f^2_{\pi NN}}{4\pi} = 0.08$) and a 20% breaking of the SU(3) symmetry, one obtains the following intervals limiting the values of the $g_{K\Lambda N}$ and $g_{K\Sigma N}$ constants:

$$-4.5 \leqslant \frac{g_{K\Lambda N}}{\sqrt{4\pi}} \leqslant -3 \quad \text{or} \quad 9 \leqslant \frac{g^2_{K\Lambda N}}{4\pi} \leqslant 20.2\,, \tag{29}$$

$$0.9 \leqslant \frac{g_{K\Sigma N}}{\sqrt{4\pi}} \leqslant 1.3 \quad \text{or} \quad 0.8 \leqslant \frac{g^2_{K\Sigma N}}{4\pi} \leqslant 1.7\,. \tag{30}$$

One notices the change of sign between $g_{\pi NN}$ and $g_{K\Lambda N}$ induced by SU(3) and the much weaker coupling of the K to Σ relative to Λ.

For the K^* coupling constants, one could in principle also rely on SU(3) to derive $g_{K^*N(\Lambda,\Sigma)}$ and $\kappa_{K^*N(\Lambda,\Sigma)}$. Here, SU(3) would link the K^* coupling constants with the ρ's. The relations are similar to Eqs. (27) and (28). If one defines:

$$G^E_{\mathrm{MBB}} = g_{\mathrm{MBB}}\,, \tag{31}$$

$$G^M_{\mathrm{MBB}} = \kappa_{\mathrm{MBB}} \cdot G^E_{\mathrm{MBB}}\,, \tag{32}$$

where, in an obvious notation, M is the ρ or K^* meson and BB the baryon pair NN or ΛN. One then obtains for the Λ:

$$G^E_{K^*\Lambda N} = -\frac{1}{\sqrt{3}} G^E_{\rho NN}(3 - 2\alpha^E_*)\,, \tag{33}$$

$$G^M_{K^*\Lambda N} = -\frac{1}{\sqrt{3}} G^M_{\rho NN}(3 - 2\alpha^M_*)\,. \tag{34}$$

And for the Σ:

$$G^E_{K^*\Sigma N} = -G^E_{\rho NN}(1 - 2\alpha^E_*)\,, \tag{35}$$

$$G^M_{K^*\Sigma N} = -G^M_{\rho NN}(1 - 2\alpha^M_*)\,, \tag{36}$$

where two coefficients $\alpha^{E,M}_*$ intervene. However, these two latter coefficients are very badly known. There is no experimental confirmation of the values predicted by SU(6): $\alpha^E_* = 0$ and $\alpha^M_* = \frac{3}{5}$. Taking these values for $\alpha^{E,M}_*$ and the strong coupling constants of the ρ adopted in the pion photoproduction section, i.e. $g_{\rho NN} = 3.51$ (corresponding to $\frac{g^2_{\rho NN}}{4\pi} = 0.98$) and $\kappa_{\rho NN} = 6.1$ (i.e. $G^M_{\rho NN} = 21.41$) as given by Eq. (17), one obtains, for the Λ:

$$G^E_{K^*\Lambda N} = -\sqrt{3}G^E_{\rho NN} = -6.08\,, \tag{37}$$

$$G^M_{K^*\Lambda N} = -\frac{9}{5\sqrt{3}}G^M_{\rho NN} = -22.25 \quad \text{or} \quad \kappa_{K^*\Lambda N} = 3.66\,. \tag{38}$$

And for the Σ:

$$G^E_{K^*\Sigma N} = -G^E_{\rho NN} = -3.51\,, \tag{39}$$

$$G^M_{K^*\Sigma N} = \frac{1}{5}G^M_{\rho NN} = 4.28 \quad \text{or} \quad \kappa_{K^*\Sigma N} = -1.22\,. \tag{40}$$

Given the degree of breaking of SU(6) (of the order of $\frac{m_\rho}{m_\pi}$!), one can be very sceptical with respect to the reality of these values. Very few authors indeed adopt these *raw* values as derived from SU(3) for the K^* and one should not be hesitant to correct them. However, there will be one property of the constants that we will not neglect, it is their *sign* (negative for $g_{K^*(\Lambda,\Sigma)N}$ and $\kappa_{K^*\Sigma N}$, positive for $\kappa_{K^*\Lambda N}$), which beyond the numerical values, are imposed by SU(3) relatively to the ρ.

We will therefore adjust the strong coupling constants of the K^* by fitting them to the differential cross sections of Figs. 18 and 19. The contribution of the K being relatively well determined (Eq. (29)), the "missing" cross section can only come from the K^*, due to the simplicity of the model which requires only a little number number of participating trajectories as it has been shown in the previous section for the pion photoproduction.

We take standard trajectory equations:

$$\alpha_K(t) = 0.7(t - m_K^2)\,, \tag{41}$$

$$\alpha_{K^*}(t) = 0.25 + 0.83t\,. \tag{42}$$

And to reproduce the data of Fig. 18, we obtain the following numerical values:

$$\frac{g^2_{K\Lambda N}}{4\pi} = 10.6\,, \tag{43}$$

$$g_{K^*\Lambda N} = -23\,, \tag{44}$$

$$\kappa_{K^*\Lambda N} = 2.5\,. \tag{45}$$

Similarly, the data from Fig. 19 allow to derive:

$$\frac{g^2_{K\Sigma N}}{4\pi} = 1.6\,, \tag{46}$$

$$g_{K^*\Sigma N} = -25\,, \tag{47}$$

$$\kappa_{K^*\Sigma N} = -1\,. \tag{48}$$

The K coupling constants are comprised in the limits defined in Eqs. (29) and (30) and the signs of the K^* constants are in agreement with those predicted by SU(6). Regarding the magnitudes of these latter constants, we see that whereas the magnetic moments κ are in relative agreement with SU(6) (for the Λ, 2.5 compared to 3.66 and for the Σ,

-1 compared with -1.22), there is a strong ratio between the electric constants (for the Λ, -23 compared with -6.08 and for the Σ, -25 compared to -3.51). Levy at al. [8] who had adopted a similar approach to determine the K^* coupling constants obtained a similar result and they used (among other things, for instance an unrealistic high value for κ_ρ of the order of 14) a multiplicative factor $\lambda \approx 2.2$ to link their fitted values to the predicted values from SU(6).

3.2. Results

The differential cross section for $\gamma p \rightarrow K^+\Lambda$ is characterized by the presence of a *plateau* at very forward angles. The analogy with the $\gamma p \rightarrow n\pi^+$ differential cross section where a sharp rise is present in this same t region is obvious. It is the same mechanism which is at the origin of these two effects, i.e. in our approach the influence of the s-channel nucleon diagram. Here, the effect manifests itself by a plateau instead of a sharp rise because the contribution of the kaon relative to the K^* is less important than the contribution of the π with respect to the ρ. Also as was seen in Fig. 5, the s-channel diagram which restores gauge invariance tends to produce a rise of width m_M^2 where M is the exchanged pseudoscalar meson, so much more collimated in the case of the pion than for the kaon. Again, the explanation of this structure does not require to introduce unphysical (over)absorption effects but arises naturally from the implementation of gauge invariance. Beyond this very forward region, the K^* gives the main contribution to the cross section. One should also notice the destructive interference between the K and K^* starting from $|t| \approx .4$ GeV^2.

This plateau does not appear for the $\gamma p \rightarrow K^+\Sigma^0$ reaction because the kaon plays a negligible role for this reaction due to the weak value of the $g_{K\Sigma N}$ coupling constant as derived from SU(3).

The photon asymmetry has been measured at E_γ=16 GeV for the two reactions $\gamma p \rightarrow K^+\Lambda$ and $\gamma p \rightarrow K^+\Sigma^0$ and is shown in Fig. 20. It is close to $+1$ over the whole t region for the two processes. This is in agreement with what is expected from a reaction dominated by a *natural* parity exchange mechanism. This clearly confirms the dominance of the K^* (spin-parity 1^-) in these two reactions and consequently the strong coupling constants found in Eqs. (44) and (47). We recall that a dominance of the kaon (unnatural parity exchange) would lead to a Σ asymmetry equal to -1.

A second polarization observable has been measured for Λ photoproduction: the recoil polarization of the Λ. It is directly accessible experimentally as the Λ is self-analyzing: the angular distribution of the decay products of the Λ signs the polarization state of the Λ. Fig. 21 shows the data with the results of the model. Again, it is the interference between the two trajectories which produces a non-zero polarization. The negative sign of the polarization comes naturally from the sign of the K^* with respect to the K. This sign has been determined by SU(3) as we have seen.

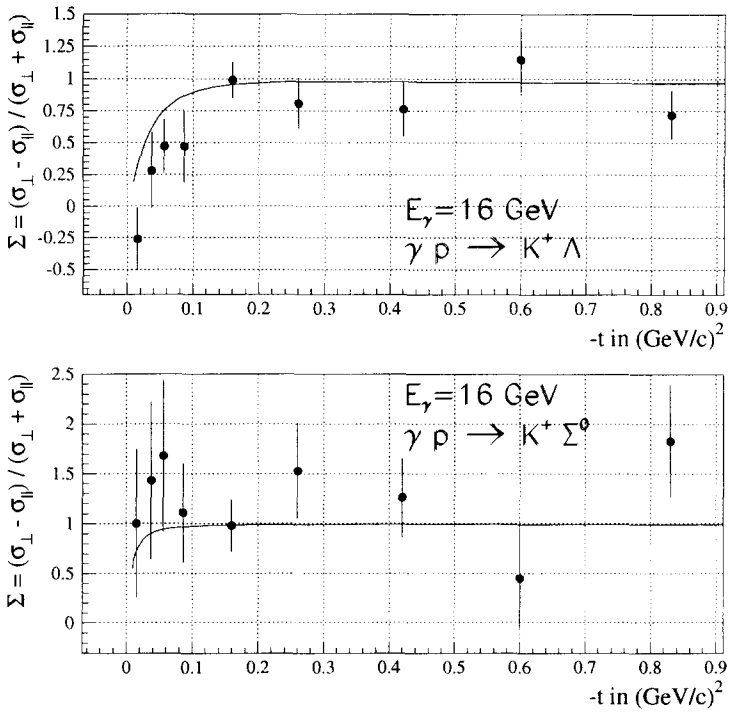

Fig. 20. Photon asymmetry for the reactions $\gamma p \rightarrow K^+ \Lambda$ and $\gamma p \rightarrow K^+ \Sigma$ for the photon energy E_γ = 16 GeV. The data are from Ref. [24].

4. Extrapolation to larger momentum transfer

Having obtained a good description of pion and kaon photoproduction observables at high energy and low momentum transfer, the question can be raised how to extend this model to larger momentum transfer. When extrapolated towards the high p_T region (large $-t$ and large $-u$), a model based on the extrapolation of linear Regge trajectories falls short to reproduce the data. One approaches the "hard" process region where the experimental data exhibit a different behavior. At scattering angles close to 90° in the center of mass frame, the differential cross-section is more or less independent of t (plateau) and scales as s^{-7} with energy. This latter behavior is simply and naturally explained by the scaling laws [43] which interpret the large p_T reactions as simple scatterings of partons. Clearly, we enter the domain of pQCD which in principle allows us to calculate and quantify exactly these interactions where the appropriate degrees of freedom are the quarks and gluons. However, these calculations are, from a practical point of view, very complex: meson photoproduction reactions imply the calculation of some thousands of Feynman diagrams at the leading order. More fundamentally, the question can be raised down to which transfer one can still apply pQCD? There is therefore a clear interest for a complementary approach which would link, extrapolate between the low and high momentum transfer regions.

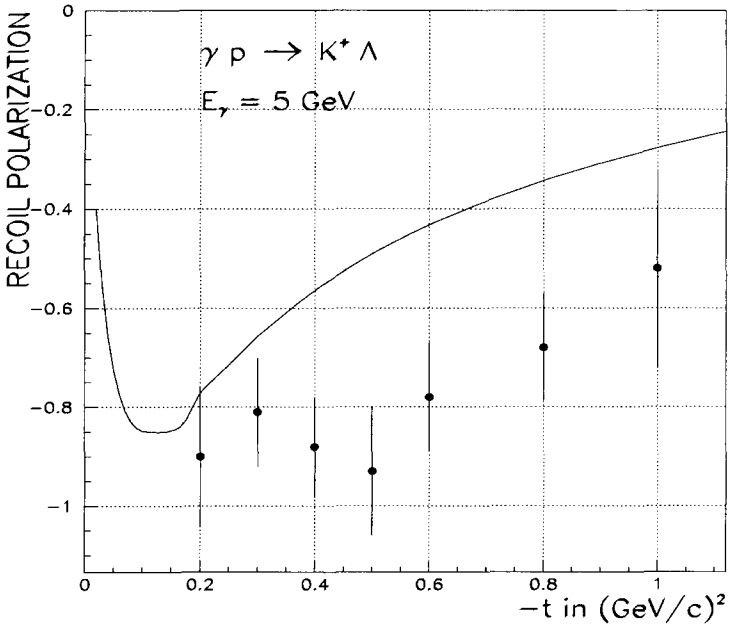

Fig. 21. Recoil asymmetry for the reaction $\gamma p \rightarrow K^+\Lambda$ for the photon energy $E_\gamma = 5$ GeV. The data are from Ref. [42].

To construct the amplitude $\mathcal{M}_{\text{hard}}$ at high momentum transfer, we apply a prescription inspired from Ref. [44] to the pion photoproduction reaction. In Ref. [44], the factorization formula was proposed

$$\mathcal{M}_{\text{hard}} = \mathcal{M}_{\text{soft}} \cdot F_3(t) \cdot F_4(t)\,, \tag{49}$$

where $\mathcal{M}_{\text{soft}}$ is the amplitude of our Regge exchange model with saturating Regge trajectories as will be explained below and $F_3(t)$ and $F_4(t)$ are the form factors of the two outgoing particles of the considered exclusive reaction ($12 \rightarrow 34$). One of the ways to reconcile at higher momentum transfer, the Regge exchange model with experiment and the counting rules is to assume that the Regge trajectories saturate at -1 for $t \rightarrow -\infty$, as was shown in Ref. [44] for the case of nucleon–nucleon and pion–nucleon scattering. For meson trajectories this result was shown [45] to follow from a QCD motivated effective interquark potential of the form:

$$\mathcal{V}(r) = -\frac{4}{3}\frac{\alpha_s}{r} + \kappa r + \mathcal{V}_0\,, \tag{50}$$

where the first term represents the short distance part of the quark-antiquark interaction and corresponds to one gluon exchange, whereas the term which is linear in r, leads to confinement (κ is known as the "string tension") and $\mathcal{V}_0$ is a constant term in the potential.

The eigenvalue equation ($E^2 = t$ as function of the angular momentum α) of the potential of Eq. (50) was inverted in Ref. [45] and the resulting equation for α was

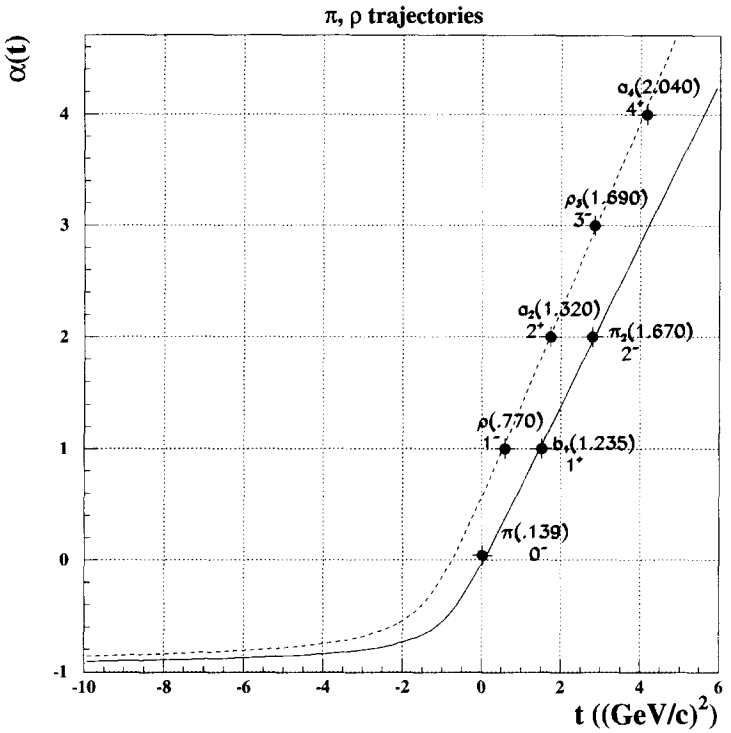

Fig. 22. Saturation of the π and ρ trajectories as in Ref. [45].

analytically continued into the scattering region ($t < 0$). This leads to the interpolating π and ρ Regge trajectories shown in Fig. 22. As one observes, they become linear as $t \to +\infty$ which reflects the bound state spectrum and saturate at -1 for $t \to -\infty$ which reflects the hard scattering (pQCD) region. The resulting hard scattering amplitude of Eq. (49) with these saturating trajectories, has a t-dependence which is much flatter than the exponential t-dependence of the "soft" model. This leads to a plateau for the differential cross section at large p_T. Moreover the differential cross section will satisfy the counting rules as shown in Ref. [44] because of the saturating trajectories and because of the form factors of the outgoing particles. Let us also remark that the high momentum transfer amplitude of Eq. (49) is normalized by the low momentum transfer amplitude.

The result of this prescription for the reaction $\gamma p \to n\pi^+$ is shown on Fig. 1 at the two photon energies E_γ = 5 GeV and E_γ = 7.5 GeV for which data exist at high momentum transfer and the predictions of our prescription are also given for E_γ = 16 GeV. Firstly, we show the results of the "soft" model with linear trajectories in the t-channel (meson exchanges) and u-channel (baryon exchanges). The u-channel model in terms of baryon exchanges will be described in a forthcoming publication. We clearly see that the extrapolation to large p_T of the model with linear trajectories cannot reproduce the plateau appearing around $|t| \approx 2.5$ GeV^2 in the differential cross section. The disagreement increases as the incident photon energy rises. On the other hand,

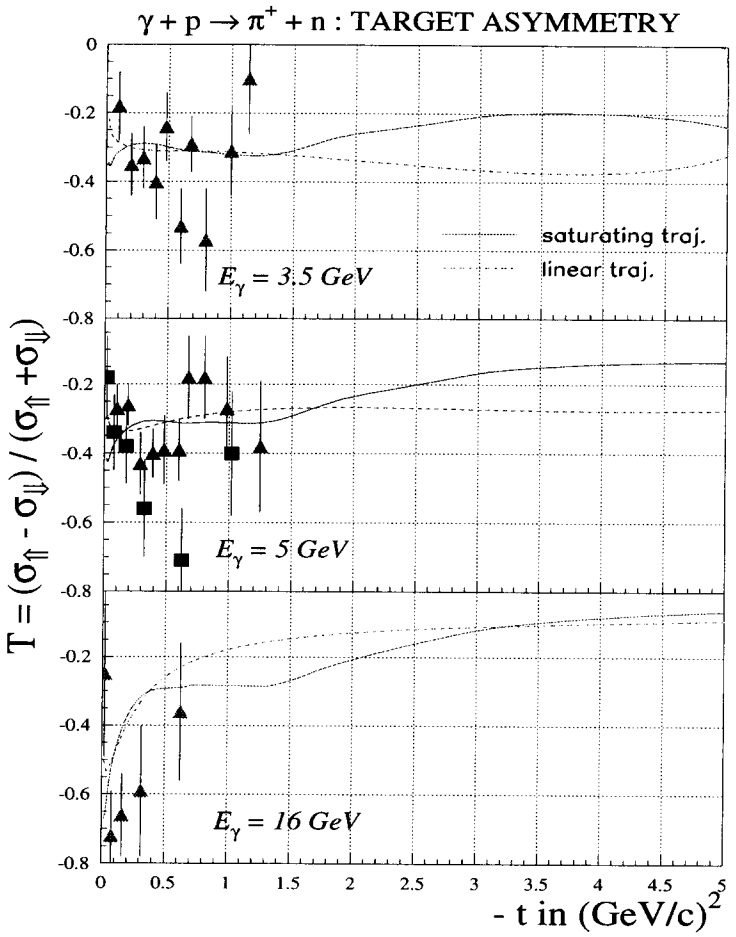

Fig. 23. Extension at large p_T of the model for the target asymmetry of $\gamma p \rightarrow n\pi^+$. Full curves: model with saturating trajectories, dashed curves: model with linear trajectories. For references to the data see Fig. 9.

the "hard" model which is obtained by extrapolating the forward amplitude to high p_T by saturating the trajectories and by using form factors for the outgoing particles (for the nucleon form factor F_4 in Eq. (49), the electric form factor was taken, whereas the unknown transition form factor F_3 was set to be 1), reproduces relatively well the shape, the energy dependence and the magnitude of the large p_T plateau. The sensitivity of the results to the precise choice of the hadronic form factors was tested by comparing the results with a calculation where the nucleon isovector Dirac form factor was used at the ρNN-vertex and the nucleon axial form factor at the πNN-vertex. We found that the apparition of the plateau at large momentum transfer does not depend upon the precise choice of the hadronic form factors but is merely due to the saturation of the trajectories.

We also present on Fig. 23 the extrapolation at large $-t$ for the target asymmetries for the reaction $\gamma p \rightarrow n\pi^+$. The extrapolation of the soft and of the hard model are to be compared with the predictions of pQCD which give a zero target asymmetry because

of Hadron Helicity Conservation [46]. It is clear that polarization observables are a very sensitive tool to study this transition domain, from partonic to hadronic degrees of freedom, from pQCD to effective hadronic models.

5. Conclusions

In this paper we have presented a Regge-based model for pseudoscalar meson photoproduction reactions at high energies and forward angles. It is gauge invariant and its parameters are fixed by the precise studies and analyses in the resonance region. Pion photoproduction reaction data are relatively numerous and permit to calibrate it. It is able to explain the main features of both charged and neutral forward pion photoproduction at high energies. Compared with existing approaches, we remarked that in the literature a good fit of charged pion photoproduction data could be obtained at high energy and at low momentum transfer however at the expense of some 30 fit parameters [29]. Our model arrives at a rather good description of the same data without invoking cuts and with no free parameters. This result is already interesting in itself. This is basically due to our implementation of gauge invariance and the use of degenerate trajectories with different phases (rotating and non-rotating) which are two new features of the present model which are responsible for the good description of polarization observables and the π^-/π^+ ratio. The same framework was then applied to the $K^+\Lambda$ and $K^+\Sigma$ reaction. We found that a description of the available cross section and photon asymmetry data leads to strong K^* coupling constants.

Besides giving an economical description of low-t data, we showed how this Regge model can be extended to interpret photoproduction data at higher momentum transfer at intermediate energies which is outside the domain of applicability of all previous Regge fit models. The extrapolation to the large p_T domain was done by introducing two additional notions: the saturation of Regge trajectories and the use of form factors. The resulting "hard" model describes reasonably well the main features of the (rare) large p_T experimental data. From a practical point of view, we have here a tool which allows to describe higher momentum transfer reactions economically. With the emergence of the new high energy, high duty-cycle accelerators like TJNAF, these largely unexplored kinematical regions will become accessible experimentally. With this respect, the model which we presented here can constitute a realistic event generator for the estimation of counting rates, background and studies of experiment feasibility. More fundamentally, we have here an approach alternative to pQCD in the transition region between soft and hard processes which is a step towards a more profound understanding of non-perturbative QCD.

The description of pseudoscalar meson photoproduction at backward angles and high energy will be presented in a forthcoming article as well as the extension of the present model to electroproduction.

Acknowledgements

This work was supported by the French Commissariat à l'Energie Atomique and in part by the EU/TMR contract ERB FMRX-CT96-0008.

References

[1] A.M. Boyarski et al., Phys. Rev. Lett. 20 (1968) 300.
[2] R.L. Anderson et al., Phys. Rev. Lett. 23 (1969) 721.
[3] R.L. Anderson et al., Phys. Rev. D 14 (1976) 679.
[4] P.D.B. Collins, An Introduction to Regge Theory and High Energy Physics (Cambridge University Press, Cambridge, 1977).
[5] J.K. Storrow, Rep. Prog. Phys. 50 (1987) 1229.
[6] M. Guidal, J.-M. Laget and M. Vanderhaeghen, Phys. Lett. B 400 (1997) 6.
[7] M. Vanderhaeghen, K. Heyde, J. Ryckebusch and M. Waroquier, Nucl. Phys. A 595 (1995) 219.
[8] N. Levy, W. Majerotto and B.J. Read, Nucl. Phys. 55 (1973) 493.
[9] J.-M. Laget, Phys. Rep. 69 (1981) 1.
[10] S. Nozawa, B. Blankleider and T.-S.H. Lee, Nucl. Phys. A 513 (1990) 459.
[11] R.M. Davidson, Nimai C. Mukhopadhyay and R.S. Wittman, Phys. Rev. D 43 (1991) 71.
[12] H. Garcilazo and E. Moya de Guerra, Nucl. Phys. A 562 (1994) 521.
[13] J.D. Bjorken and S.D. Drell, Relativistic Quantum Mechanics (McGraw Hill, New York, 1964).
[14] R. Machleidt, K. Holinde and Ch. Elster, Phys. Rep. 149 (1987) 1.
[15] Particle Data Group, Phys. Rev. D 50 (1994) 1173.
[16] M.G. Olsson and E.T. Osypowski, Phys. Rev. D 17 (1978) 174.
[17] L.M. Jones, Rev. Mod. Phys. 52 (1980) 545.
[18] J.K. Storrow, *in* Electromagnetic Interactions of Hadrons, Vol. 1, ed. A. Donnachie and G. Shaw (Plenum, New York, 1978).
[19] A.C. Irving and R.P. Worden, Phys. Rep. 34 (1977) 117.
[20] F. Henyey, G.L. Kane, J. Pumplin and M.H. Ross, Phys. Rev. 182 (1969) 1579.
[21] M.H. Ross, F. Henyey and G.L. Kane, Nucl. Phys. B 23 (1970) 269.
[22] H. Burfeindt et al., Phys. Lett. B 33 (1970) 509.
[23] D.J. Sherden et al., Phys. Rev. Lett. 30 (1973) 1230.
[24] D.J. Quinn et al., Phys. Rev. D 20 (1979) 1553.
[25] H. Genzel et al., Nucl. Phys. B 92 (1975) 196.
[26] C.C. Morehouse et al., Phys. Rev. Lett. 25 (1970) 835.
[27] Z. Bar-Yam et al., Phys. Rev. Lett. 19 (1967) 40.
[28] A.M. Boyarski et al., Phys. Rev. Lett. 21 (1968) 1767.
[29] M. Rahnama and J.K. Storrow, J. Phys. G: Nucl. Part. Phys. 17 (1991) 243.
[30] R. Anderson et al., Phys. Rev. D 1 (1970) 27.
[31] R.L. Anderson et al., Phys. Rev. D 4 (1971) 1937.
[32] P.S.L. Booth et al., Phys. Lett. B 38 (1972) 339.
[33] H. Bienlein et al., Phys. Lett. B 46 (1973) 131.
[34] M. Deutsch et al., Phys. Rev. Lett. 29 (1972) 1752.
[35] A.M. Osborne et al., Phys. Rev. Lett. 29 (1972) 1621.
[36] R. Adelseck and B. Saghai, Phys. Rev. C 42 (1990) 108.
[37] R. Williams, C.R. Ji and S.R. Cotanch, Phys. Rev. C 46 (1992) 1617.
[38] T. Mart, C. Bennhold and C.E. Hyde-Wright, Phys. Rev. C 51 (1995) 1075.
[39] J.C. David, C. Fayard, G.H. Lamot and B. Saghai, Phys. Rev. C 53 (1996) 2613.
[40] J.F. Donoghue and B.R. Holstein, Phys. Rev. D 25 (1982) 2015.
[41] A.M. Boyarski et al., Phys. Rev. Lett. 22 (1969) 1131.
[42] G. Vogel et al., Phys. Lett. B 40 (1972) 513.
[43] S.J. Brodsky et G.R. Farrar, Phys. Rev. Lett. 31 (1973) 1153.
[44] P.D.B. Collins and P.J. Kearney, Z.Phys. C 22 (1984) 277.
[45] M.N. Sergeenko, Z.Phys. C 64 (1994) 315.
[46] S.J. Brodsky and G.P. Lepage, Phys. Rev. D 24 (1981) 2848.